Magnetic Resonance Wireless Power Transfer Systems Sensing and Applications

A Master's Thesis
Submitted to the Faculty of the
Escola Tècnica d'Enginyeria de Telecomunicació de Barcelona
Universitat Politècnica de Catalunya
by
Armand Mollà Garcia

In partial fulfilment
of the requirements for the degree of
MASTER IN ELECTRONICS ENGINEERING

Advisors:
Kaushik Chouwdhury, Sandra Bermejo

January 31, 2019

Northeastern University

To my family, for their effort, without which it would have been impossible, and to everyone in Boston and the GENESYS Lab who have made me feel like at home.

Abstract

Magnetic Resonance (MR) Wireless Power Transfer (WPT) is a specific case for the well known inductive coupling principle where energy is transmitted from a transmitting coil to a receiving one without the need of any wires. This technology brings enhanced capabilities and offers the possibility to create cutting edge wireless charging systems. The objective of this thesis is to understand and develop the elements needed to build a MR WPT system capable of charging multiple wearable devices placed over a large surface. The focus is put in current and voltage sensing at high frequency for system monitoring; power amplifier topology design to maintain good performance across a range of load values; and the beamforming and energy hopping applications validation to deal with charging area coverage and transmission distance issues. The results show how the presence of a receiver can be detected from the current change measured at the transmitter, as well as voltage measurements are used as redundant information for system failure detection; a class E power amplifier has been successfully designed to operate with loads that differ 1 order of magnitude from each other; beamforming and energy hopping simulation environments have been set, and experiments have shown a 50% improve in the received signal strength with the use of beamforming, while the enrgy hopping phenomena has been empirically demonstrated for up to four hops along a planar array of coils. A solid basis has been set to allow further development of the aimed wireless charging surface.

Contents

List of Figures

List of Tables

Acronyms list

AC Alternating Current

ADC Analog to Digital Converter

BF Beamforming

BOM Bill Of Materials

DC Direct Current

EPS Electrical Power Subsystem

FET Field-Effect Transistor

GaN Gallium Nitride

MCU Micro Controller Unit

MEMS Micro-Electro-Mechanical System

MI Magneto-Inductive

MOSFET Metal-Oxide-Semiconductor Field-Effect Transistor

MR Magnetic Resonance

NSF National Science Foundation

NU Northeastern University

PCB Printed Circuit Board

PWM Pulse Width Modulation

RF Radio Frequency

RFID Radio Frequency Identification

RMS Root Mean Square

SI International System of units

SMA SubMiniature version A

UAV Unmanned Aerial Vehicle

UPC Universitat Politècnica de Catalunya

WPC Wireless Power Consortium

WPT Wireless Power Transfer

WSN Wireless Sensor Networks

ZCS Zero Current Switching

ZVS Zero Voltage Switching

Chapter 1

Introduction

WPT is a field that is supposing a revolution in many industrial and consumer applications for seamlessly charging batteries or powering devices without the need of any cord or connection.

Inductive coupling is the most common technology used for close proximity and high power applications. Then, the specific case of MR adds some complexity to the system, but offers the possibility of enhancing several features. The main focus of this thesis has been on the MR based WPT systems for consumer applications, more specifically, for the charging of wearable devices.

This work has been carried on at professor Kaushik Chowdhury's GENESYS lab in Northeastern University (NU) in Boston, USA. The laboratory's expertise in the WPT world was on Radio Frequency (RF) energy harvesting because of their previous reaserch studies on powering nodes in Wireless Sensor Networks (WSN) [9] [10]. With the aim of working on applications with higher power needs, inductive coupling-based power transfer was decided to be the next research topic.

This project coincided with the period of time when the laboratory wanted to gain expertise in the field and build the first prototypes. It was decided to pursue the idea of a large charging surface that would transfer power to several wearable devices at the same time as an ambitious goal. All the challenges, difficulties and achievements along the way of reaching this objective would help maturing the knowledge around this chosen technology.

Consequently, the purpose of this thesis has been to understand and develop the hardware elements that would compose the aimed system, as well as testing alternative implementations that could enhanced the system's features. A solid theoretical and experimental basis should be created towards further development. Theoretical analysis, simulations and physical implementation were required in order to validate all the ideas to be potentially included in the final application.

The requirements or characteristics to be taken into account along the development of this project were:

- The aimed system has to be capable of simultaneously charging or powering multiple

devices placed in any position over a big surface such as a conference table.

- The final product could eventually be commercialized, so feasibility and cost have to be always in mind.
- The charging action has to be homogeneous all over the surface.
- This system should should be as invisible as possible to the user, being placed at the other side of the surface. Then, the minimum charging distance should always be more than 2 cm.
- The devices to be charged might not have the same power requirements.
- The designed system should be easily scalable to different scenarios depending on the surface that is to be covered.
- External elements to the surface such as sensors or cameras should be avoided as much as possible.
- The proposed techniques or technologies to be included as system improvements have to be verified with simulations and experiments if possible.

The technology chosen for this application has been the 6.78 MHz MR, and the biggest challenges were found to be related with the system's monitoring and the high frequency, high power signal handling. For this reason, this work is divided in two main parts:

1. What can be named as the functional block, the largest one in this thesis, is integrated by the sensing and amplifier chapters, related to these two mentioned challenging issues. These are basic system elements to be implemented to guarantee good performance and allow the inclusion of additional features for system improvement.
2. The second part is composed by the beamforming and energy hopping chapters, which is called the applications block. These are two specific solutions for performance limitations a basic WPT would have. They are studied and tested for further development and their future inclusion in the aimed charging system.

Chapter 3, the most extensive part in this thesis, consists of the development of a sensing circuit to detect signal characteristics on the transmitter's side. The proposed sensing approach allows gathering valuable information for receiver detection and transfer performance. The design, circuit schematics simulations, components selection and PCB layout design, and testing are presented. Chapter 4 works on the power amplifier required for the transmission, believed to be the most important hardware element in the system structure, and critical for the system performance. A simple and improved design is presented for operation under variable load conditions.

Then, on the applications side, Chapter 5 deals with the MR Beamforming (BF) approach for solving surface coverage challenges. Simulation and experimentation complement its theoretical study. Chapter 6 presents a more novel approach for dealing with

long distance transmission with simpler hardware. In the same way as for the beamfoming, its advantages and drawbacks are analyzed through COMSOL Multiphysics simulations and experiments to set a good basis to continue with its development in the future.

During the project development, a continuous supervision by the advisor Professor K. Chowdhury through weekly presentations has been performed. They would work as a follow up for the project and to take decisions about next steps or discuss which of the new approaches found would be further studied.

Summarizing, this thesis opened the doors towards a topic totally new for the GENESYS lab, and a good basis has been set by working on the first steps towards a state-of-the-art wireless power charger. It has been a very useful project to introduce the team members to several MR WPT alternatives and give them the possibility to continue with their development after having designed and implemented simulations and experiments useful for this purpose.

Chapter 2

Background

Many developments and theories around the transmission of electrical energy appeared during the 19th century. In 1826, Ampère's circuital law showed that electric currents produce a magnetic field around the conductors. Faraday's law of induction, described in 1831, predicted how a magnetic field interacts with an electric circuit to produce an electromotive force.Then, in the 1860s, the well known Maxwell's equations established a theory that unified electricity and magnetism to electromagnetism, which would give a concise explanation to the phenomena observed before by Ampère and Faraday. After that, the Poynting's theorem would describe the power across an area within electromagnetic radiation and allow the correct analysis of wireless power transfer systems.

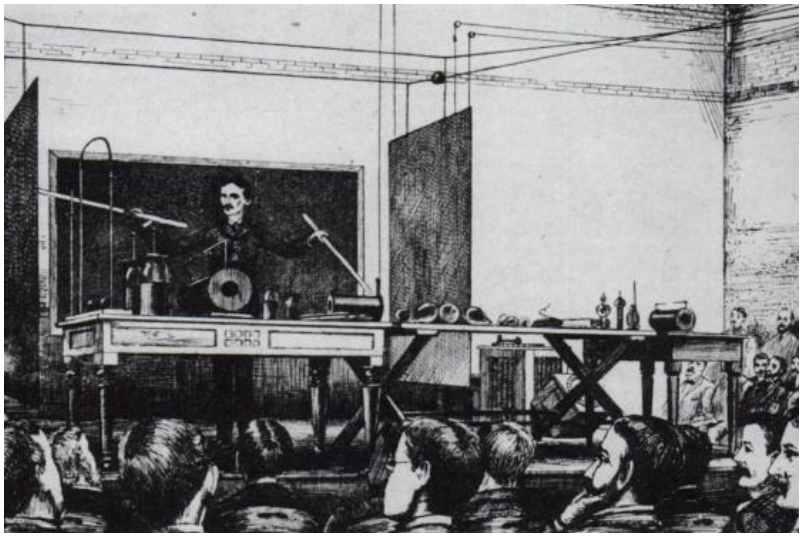

Figure 2.1: Nikola Tesla demonstrating wireless transmission by "electrostatic induction" [1]

The concept of WPT was used by Nikola Tesla in 1890 when he experimented with power transmission using inductive and capacitive coupling with the so called Tesla coils, which generated high Alternating Current (AC) voltages. When investigating on the near-field power transmission, he found that he could extend the range of the transmission by using LC resonant circuits in both transmitter and receiver if tuned to the same resonating frequency. He conducted several public demonstrations where he lit Geissler tubes and

incandescent light bulbs across a stage, as depicted in Figure 2.1.

Nowadays, WPT is a generic term for a number of different technologies for transmitting energy by means of electromagnetic fields.The technologies differ in the distance over which they can transfer power efficiently, whether the transmitter must be directed towards the receiver, and in the type of electromagnetic energy they use: time varying electric fields, magnetic fields, radio waves, microwaves, infrared or visible light waves [11].

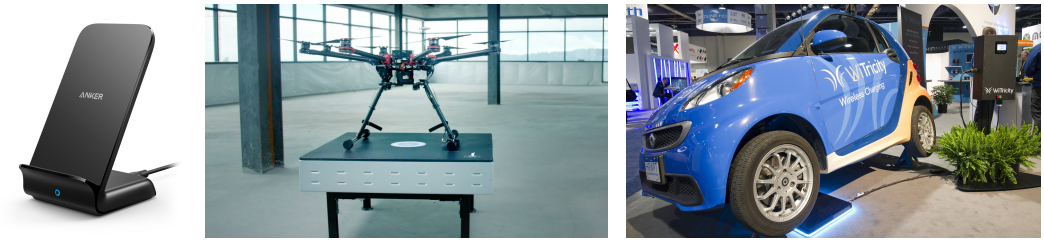

(a) Qi phone Fast Charger (b) Drone charging platform (c) Electric car wireless charger

Figure 2.2: Some examples of applications and products

More and more commercial off-the-shelf products are starting to use ore include WPT technology, and a lot of effort is being put on the research side, exploring the many possibilities these technologies might bring. The most common and popular devices are the phone chargers, available in many formats and integrated in different places, such as on desktop towers or cars. Then, more powerful and challenging products are being developed and will soon be very common. Unmanned Aerial Vehicle (UAV) charging platforms and electric car wireless chargers, like the ones seen in Figure 2.2, are in advanced stages of development.

2.1 WPT types and focus

When we talk about WPT, two main categories can be identified, the near field or non-radiative, and the far-field or radiative. In the non-radiative techniques, power is transferred over short distances by magnetic fields using inductive coupling and by electric fields using capacitive coupling. In radiative techniques, power is transferred by means of electromagnetic radiation, like laser or microwave beams. An example of a far-field WPT application is the RF energy harvesting, a hot research topic these days. Figure 2.3 shows this classification.

The most commonly used WPT technology for cordless device and battery charging is the inductive coupling, in the near-field category. It is the case of the Qi standard, widely used for wireless phone charging. Then, a specific case can be identified within this category, the resonant inductive coupling, also called MR. In this mode, some features are enhanced, including the range of the transmission, reason why some call it a mid-field transmission. MR is seen as a step forward after the conventional inductive coupling by many although it is still facing many challenges to become commercially available. The creation of the AirFuel alliance is an example of this trend, an organization which is

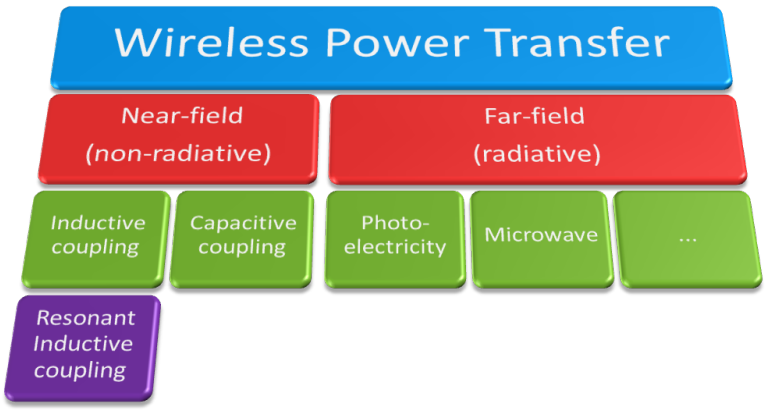

Figure 2.3: WPT technology classification

trying to provide an alternative to the Qi standard using the resonant technology. The main characteristic of inductive and MR technologies is the use of simple coils that act as transmitter and receiver. In the far-field, the use of antennas is required. Section 2.2 talks in more detail about the similarities and differences between these two modes, the ones around which this thesis works.

2.2 Inductive Coupling and Magnetic Resonance

Inductive coupling is a well established technology that is monopolizing the cordless portable device charging. And, if we talk about inductive coupling, it is a must to talk about the Qi standard, developed by the Wireless Power Consortium (WPC), a collaborative standards development group created in 2008. When talking about inductive coupling, then, Qi standard is usually used as the reference, providing the most mature and robust way of using the technology [12].

Inductive coupling has become well used for its reasonably simple technology that achieves good efficiency at very short distances. The basic principle that makes it work relies on the tight coupling between two coils (the transmitter and the receiver). If most of the magnetic flux generated by an AC current at the transmitter travels through the receiver, a proportional current is going to be induced there, achieving the wireless transfer. Achieving tight coupling requires some conditions the system's configuration has to meet: very short distance from transmitter to receiver, and similar dimensions of the coils.

Then, the inductive coupling technology brings some great features such as the simplicity, having a well developed standard, good efficiency, and the ability to avoid interference from other wireless devices or signals since it is possible to use low frequencies without having a negative impact on the performance (100 to 200 kHz in the case of the Qi standard). On the other hand, this simplicity and short range to maintain the tight coupling condition make this technology have evident limitations. There is no positioning freedom

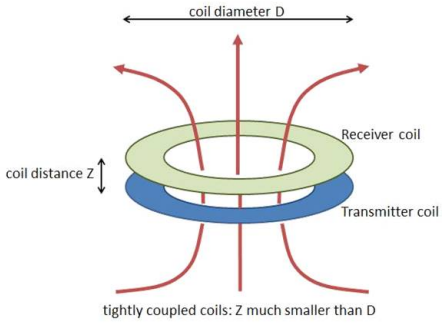

Figure 2.4: Scheme depicting the tight coupling between coils

for the receiving device over the transmitter (in any direction), the charging distances are very short and there exists only one-to-one transmission. These benefits and limitations are summarized in Figure 2.5.

Figure 2.5: Inductive coupling features(blue) and limitations(red)

Alternatively, the MR approach tries to solve the previously mentioned limitations to provide more flexible and useful applications. Now, the power transmission relies on loosely coupled coils, where only a few lines of the magnetic flux generated at the transmitter travel through the receiver. This allows transmitting over longer distances, having different sizes for transmitter and receiver coils and, potentially, the possibility of charging several receivers at the same time. An example of a well known application that uses a loosely coupled configuration is Radio Frequency Identification (RFID).

On the circuital side, resonance is achieved by adding a resonating capacitor in series to both the transmitting and receiving coil, which are treated as inductors in the circuital analysis. The series LC configurations resonate at the transmission frequency, the one provided by the AC voltage source on the transmitter side. The schematic is shown in Figure 2.6b, where the resonator capacitors can be seen. The resistors model the series resistance of each coil.

A big benefit that MR would bring is the possibility of building charging surfaces for several devices without requiring a huge amount of transmitting coils to build it. The

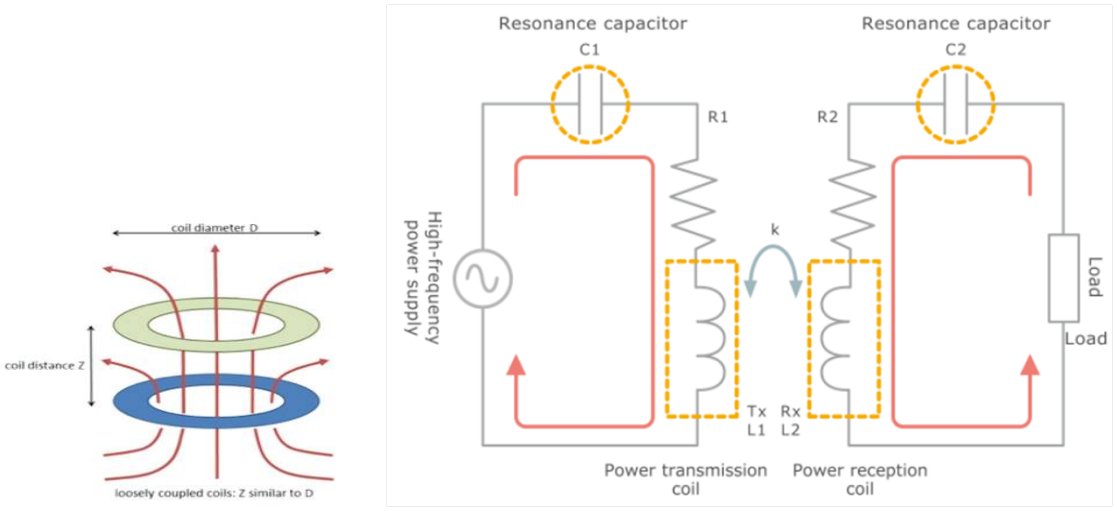

(a) Loosely coupled coils (b) Resonant mode circuit schematic

Figure 2.6: MR loosely coupled coils and circuit schematic

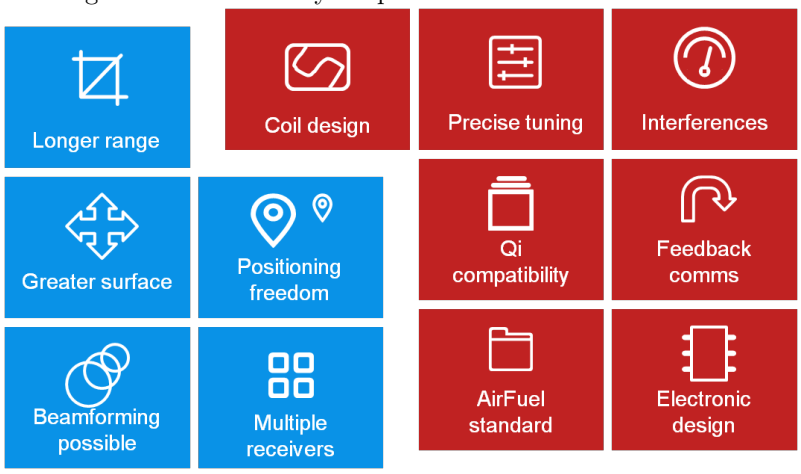

Figure 2.7: Resonant mode opportunities(blue) and challenges(red)

multi-device charging surface is an idea that has been pursued by many in the recent years, and fewer bigger coils would make it a more realistic objective. In the same direction of achieving big charging surfaces that allow placement freedom, the technology would allow a specific kind of beamforming, about which more emphasis is going to be put further in this thesis.

Despite all the benefiths though, many challenges appear at the time systems that use MR have to be built, and even more when they have to reach the market. The technology is not compatible with the existing Qi compliant devices, thus, another standard should achieve being widely deployed and guarantee all MR-based devices meet the requirements specified by the regulations (AirFuel is trying to become that standard [13]). Precise tuning is needed for the resonance condition, and higher frequencies have to be used in order to achieve reasonable efficiency levels, then, interference with and from other devices and systems becomes an issue. The higher frequencies in the MHz range, combined with power, make the electronic design of the system complex as well. Additionally, the feedback

communication from receiver to transmitter cannot be done in the backscattered way the Qi standard does, so it requires an extra communication link, which adds complexity to the system. All this is summarized in the diagram in Figure 2.7.

2.3 Magnetic Resonance WPT Systems

2.3.1 System Overview

Now that we know in which segment of the wireless power transfer world our focus is on, it is the turn for the elements that compose these systems. The simplest case to understand is the one transmitter to one receiver scenario, with one coil each, as shown in the block diagram in Figure 2.8.

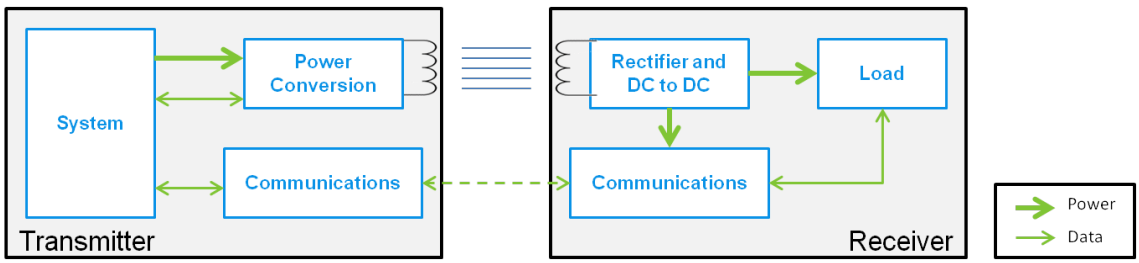

Figure 2.8: MR generic system block diagram

On the transmitter side, the *System* block represents the rest of the device or micro controller, the one that takes the decisions and is connected to a power source. The *Power Conversion* block is the one passing the power to the transmitting coil (LC resonant configuration) with the right frequency and amplitude, and, finally, a communications block is responsible for gathering and sending data for feedback and control purposes.

On the receiver side, we find a coil which is going to receive the power and send it to a rectifier and, most likely, to a DC to DC converter as well, to feed the load. The load is going to be a battery, in most of the cases, or an actuator, or directly a micro controller, depending on the function of the system (batteries are not used in biomedical applications for example). We also find a communications unit that is going to exchange information with the transmitter through another link (RF Bluetooth link, for example). Note that this block is also powered with the energy received through the transfer. The configuration at the receiver is not complex, but a good power management is required in order to obtain adequate efficiency levels.

2.3.2 Transmitter critical blocks

The power conversion block in the transmitter is, from the circuit and electronics point of view, the most complex and challenging one to build. The block diagram in Figure 2.9 shows this part in more detail.

Apart from the capacitor-coil resonator, that acts as the ”antenna” of our system, there are two important blocks that need to be thoroughly designed and implemented.

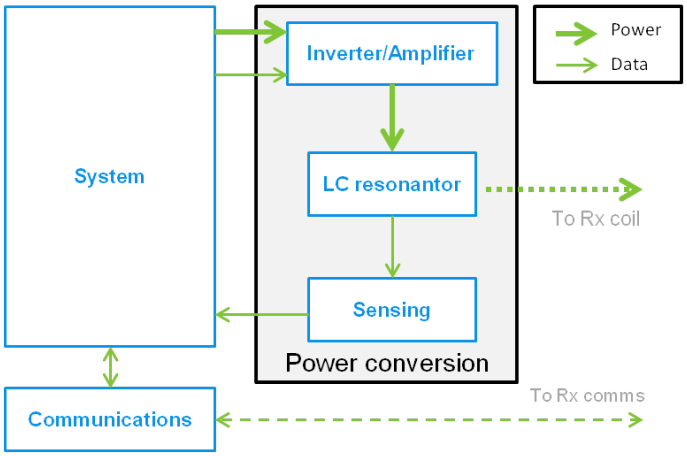

Figure 2.9: Transmitter block diagram

The first one is the amplifier, also called inverter, since its function is to convert the input Direct Current (DC) voltage from the power source to an AC power signal at the resonance frequency. Together with the amplifier, an oscillator at the transmission frequency is also needed. Regarding the implementation of these amplifiers, there are many different kinds but, since this is a power transfer application, the typologies used are the ones that can provide the highest efficiency. Thus, the amplifiers used in WPT applications are, usually, switching amplifiers, such as the so called class D or class E amplifiers. Chapter 4 describes tasks performed around this specific block and gets into more detail about the amplifiers' characteristics, performance, and structure.

The *Sensing* block is also an important and challenging element in the system, and its complexity will depend on frequency, power and system structure. It is particularly complicated since the measurements needed have to be made at the transmitting coil and, there, the signal has relatively high power (from a few Watts to tens of Watts) at the same time as high frequency (MHz range). The elements that carry information there are the voltage and current amplitudes and the phase difference between them. The tasks described in Chapter 3, one of the main parts of this thesis, are exclusively related to this block.

Chapter 3

Multi-coil Sensing Circuit

As presented in Section 2.3, sensing to acquire information for control and feedback purposes is an important function the transmitter has to handle in the MR WPT context. Additionally, this sensing becomes even more crucial when the scenario aimed is more complex than only one transmitter and one receiver or techniques such as beamforming or energy hopping are to be implemented.

In particular, the aim of our MR wireless charger is to transfer power through a 6.78 MHz signal to several devices that can be positioned in any position over a large surface (like a big conference table, for example). Here, apart from controlling each transmitting coil for the correct performance of the power transfer, there is the need of detecting when and in what position the receiving devices are placed.

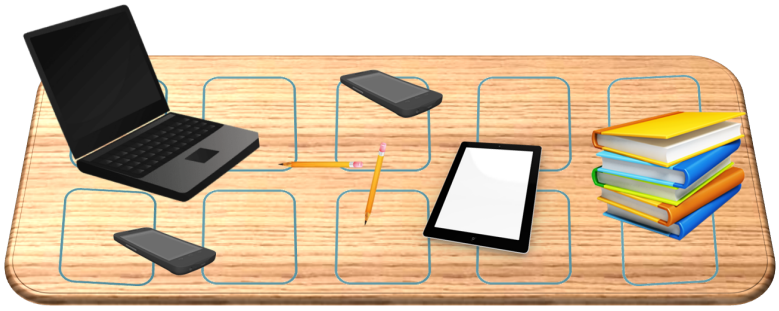

Figure 3.1: Scheme of the aimed desk scenario and MR wireless charging

Some ideas such as the use of millimeter wave radars, image detection through cameras, infrared sensors or pressure sensors have been explored. These options, nonetheless, add big complexity to the system and still have drawbacks when having to distinguish what each object is, whether it is potentially chargeable or detecting several objects at the same time.

Our approach to start solving this detection dilemma relies on the voltage and current changes experienced at the transmitting coils to detect when a receiving coil able to draw power appears. This way, the system can detect different devices that can be charged while not reacting to other objects. The main advantage of this solution is its compactness and

integration with the transmitting hardware. No additional elements, devices or computing units are needed, the coil directly acts as a sensor.

Figure 3.2 shows a basic schematic for a one transmitter and one receiver scenario.

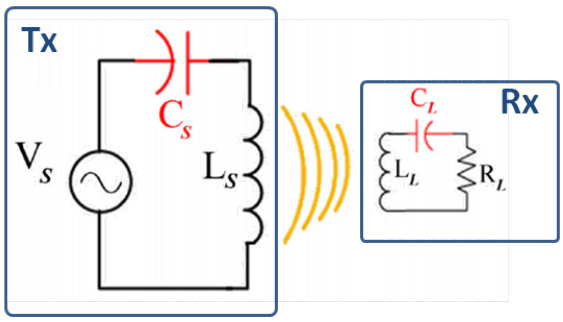

Figure 3.2: One transmitter to one receiver magnetic resonance configuration schematic.

In the same way the transmitter produces a change on the receiver's parameters inducing a current that is going to flow through the load (Equation 3.1), the receiver's presence has an impact on the transmitter (Equation 3.2).

$$I_L \left(R_L + j\omega L_L + \frac{1}{j\omega C_L} + z_L \right) = j\omega M I_S \tag{3.1}$$

$$V_s = I_s \left(j\omega L_s + \frac{1}{j\omega C_s} + z_s \right) = j\omega M I_L \tag{3.2}$$

Note that, when working at the resonance frequency, the terms $j\omega L$ and $\frac{1}{j\omega C}$ cancel each other and disappear from the equations.

See how, from Equation 3.2, it can be understood how the mutual coupling between coils, load, and the induced current on the transmitter side have an impact on the transmitter's voltage and current.

Then, apart from detection purposes, monitoring is also important in these sort of applications. The power flowing into the transmitting coil is also a parameter of interest to be measured since the amplifier's performance is never a 100%. To measure the AC power at a frequency of several MHz, other than voltage and current amplitudes, the phase difference between them is also important to be measured. Equation 3.3 shows the relationship to calculate the real power in the transmitting coil [14].

$$P_{coil} = V_{coil} \cdot I_{coil} \cdot cos(\phi) \tag{3.3}$$

Being the current and voltage the Root Mean Square (RMS) values and ϕ the phase difference between them.

The described sensing configuration sets the basis for future improvements and additional features. Other issues such as RFID tags detection (because of the use of similar frequencies, RFID tags could be damaged), or distinguishing receivers placed very close or on top of each other are more complex, and would be solved in future stages of the sensing challenge. The detection of objects between transmitting coils is possible even though it

is more complex, but can be achieved with the combination of feedback from several coils and, possibly, with the use of machine learning algorithms. This is also a next step the group has in mind.

3.1 Sensing circuit requirements

The sensing circuitry to be added to the system would be placed between the EPC9128 class D power amplifier and the LC resonator by nuCurrent on the transmitter side [15]. The parameters to be detected were current and voltage amplitudes and the phase difference between them. These parameters would allow calculating the real power that is being sent through the transmitting coil and help analyzing the system efficiency. The amplitudes of voltage and current would tell about the presence of a receiving device placed over the transmitter and help finding anomalies. The receiver used for the tests was the EPC9515, capable of gathering up to 10 Watts and providing a 5 Vdc voltage at its output [16].

At the time of designing the sensing circuits, several requirements had to be taken into account:

- The sensors have to have the minimum impact possible on the performance of the circuit
- Power consumption has to be kept as low as possible. Ideally, no additional power supply would be needed if only passive components were used.
- Sensors simplicity and low cost is a must since the measurements have to be taken in every transmitting coil.
- The designed board should be independent to the application so it can be used in other projects that involve MR WPT.
- Highly configurable boards are preferred in order to explore and test different options easily.
- The outputs have to be readable from an Arduino or RaspberryPi to simplify the testing and emulate the theoretical final application, where they should be read from a Micro Controller Unit (MCU).
- Board dimensions are not critical at this point, but the sensors configuration must allow miniaturization.

In the following sections, the design of a PCB board that is placed between an amplifier and a transmitting coil is described. Two versions of the board have been manufactured so far and, the ideas, achievements and lessons learned for each of the PCBs are reviewed here.

3.2 Sensing Printed Circuit Board v1

The first version of the sensing PCB was intended to be a fully configurable board, with the main purpose of testing different sensors for voltage and current amplitude detection so we could determine which ones offered the best performance. This board was designed with the need of a second version already in mind. The schematic, PCB layout and Bill Of Materials (BOM) can be found in Appendix A.1.

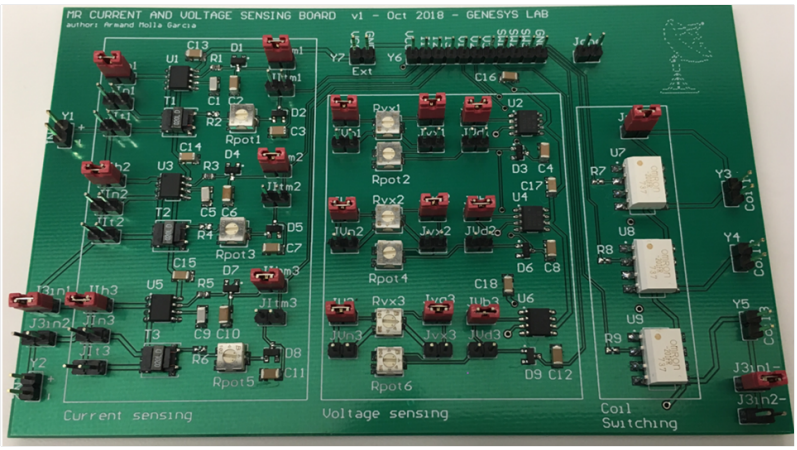

Figure 3.3: Picture of the first version of the sensing board for up to three transmitters.

3.2.1 Features and elements

All the features and possibilities offered by the board are listed below:

- Connections to amplifiers and coils through jumper wires.
- Configurable by means of manual jumpers.
- Two options for each voltage and current amplitude detectors.
- Possibility to use one shared sensing circuit for up to three coils using optocouplers as switches.
- Possibility to connect either one shared amplifier or two different amplifiers to drive the coils.
- Most of the resistors for voltage dividers or gain determination were potentiometers to allow adjustment.
- Most of the elements and sensors in the board could be bypassed for better debugging of the PCB elements.
- Rectifiers implemented with the simplest diode-capacitor configuration.
- Header for direct connection to an Arduino to monitor the measurements.

- Separate pins for VCC connection in case the MCU's 5V supply was not enough for the board.

The board's schematic is shown in Figure 3.8. All the listed features can be seen there. The red boxes identify each of the sections of the board.

The next sections explain, one by one, the configuration and reason for each of the parts included in the design.

3.2.1.1 Current amplitude detection

The current amplitude is the most important parameter to be detected in our system. It tells when there is a receiver charging over the transmitter and its value is different depending on how much power that receiver is drawing.

The main challenge with the current sensor is that it has to be placed in the circuit, in series with the coil, it cannot just be a high impedance connection to a certain node. The method chosen must not distort the original signal or have a negative impact on the efficiency. The high frequency of 6.78 MHz makes it challenging task as well.

Three different sensors were chosen to be compared: a current sensor based on the Hall effect; a detector that would rely on a transformer; and a measurement through the determination of the voltage drop at a known small resistor. The Hall sensor selected would be an ACS712 that would directly output a proportional voltage to the current flowing to the coil [17]. It was the simplest approach, with the drawback of being an active sensor, thus, needing to consume some power to work.

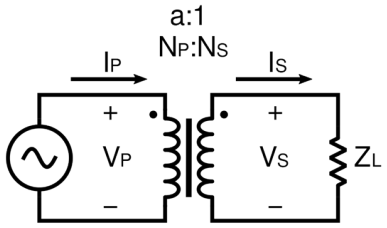

Figure 3.4: Transformer schematic and nomenclature from the circuit point of view

The second sensor would be a transformer CST7030 20:1 by Coilcraft [18]. It would be the preferred solution a priori for being a passive implementation for the sensor. At the secondary winding, a voltage proportional to the current flowing through the primary winding would be induced, then, the amplitude of this voltage would provide the current information desired. A rectifier would be needed before reading the voltage. The classical analysis of the ideal transformer behavior is explained through the following equations.

By Faraday's law of induction:

$$V_P = -N_P \frac{d\Phi}{dt} \tag{3.4}$$

$$V_S = -N_S \frac{d\Phi}{dt} \tag{3.5}$$

And by conservation of energy:

$$I_P V_P = I_S V_S \tag{3.6}$$

Then, combining these three equations, we obtain the well known characteristic for ideal transformers:

$$\frac{V_P}{V_S} = \frac{N_P}{N_S} = \frac{I_S}{I_P} \tag{3.7}$$

V means voltage, I is current, and N is the number of turns in a winding.

Finally, by applying Ohm's law on the secondary side, and combined with the ideal transformer's equations:

$$I_S = \frac{V_S}{Z_L} \tag{3.8}$$

then,

$$I_P = \frac{V_S I_S}{V_P} = \frac{V_S N_S}{N_P Z_L} \Rightarrow V_S = Z_L \frac{N_P}{N_S} I_P = k I_P \tag{3.9}$$

being k a constant factor.

It is shown, here, how the induced voltage on the secondary winding is proportional to the current on the primary.

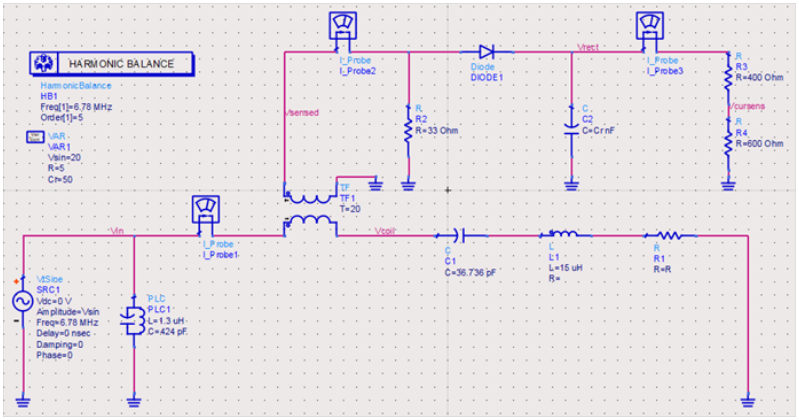

Figure 3.5: Simulated schematic to verify the transformer approach performance

After understanding the basic principle behind the transformer approach method for current magnitude measurement, the circuit to be used was simulated. Figure 3.5 shows the simulated circuit schematic. For this simulation, different arbitrary AC currents flowing through the transmitting path (Figure 3.6a) would be provoked by changing the value of the transmitting load (R1), then, each of the voltages would be measured on the other side (Figure 3.6b).

The results verify the behavior predicted from the equations. Different currents can

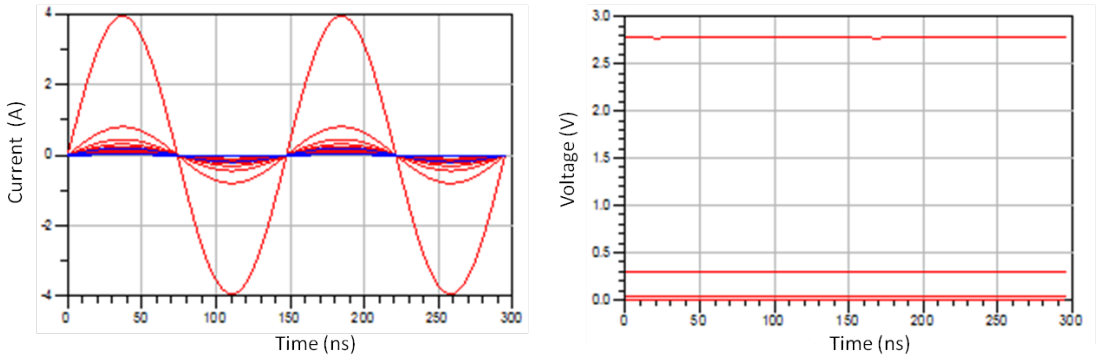

(a) Different arbitrary input AC currents through the primary winding

(b) Sensor's output DC voltages proportional to each of the input currents

Figure 3.6: Transformer-based current sensor simulation results

be translated to several proportional voltages on the other side of the transformer. The simulated rectifying scheme also performed as desired.

The last approach would work together with the voltage sensor and, with the help of jumpers, the point at which the voltage was measured could be chosen to be before and after a small resistor. With that voltage drop calculation, the current flowing through it would be calculated. The main drawback of this measurement, and what made it the least appealing solution, was the need of a resistor in the middle of the power circuit. Rvx is its name in the schematic (see Figure 3.8) and it was chosen to be a 1 to 100 Ω potentiometer so the most suitable value could be selected.

3.2.1.2 Voltage amplitude detection

The voltage detection is the simplest part on the sensing board with the use of voltage dividers with big resistors in order not to drain power. This voltage detector is the same that would be used for the third current measurement method explained in the previous section. It would be used to detect anomalies in the system behaviour as well since the amplifiers used provide a fixed voltage which does not depend on the receiver load effect.

Two different configurations were designed: one would simply use a voltage divider before a rectifier, and the second configuration would isolate the rectifier from the circuit with a voltage buffer implemented with an operational amplifier (OPA350 by Texas Instruments) [19]. This would help in case the first approach had a negative impact on the circuit behavior.

For the voltage buffer, the transfer function is really simple since it just "copies" the output from the input and Vout = Vin. The voltage divider transfer function is:

$$V_{out} = \frac{V_{in} R_2}{R_1 + R_2} \tag{3.10}$$

Potentiometers were used instead of R1 and R2 in the voltage dividers to make their ratios adjustable.

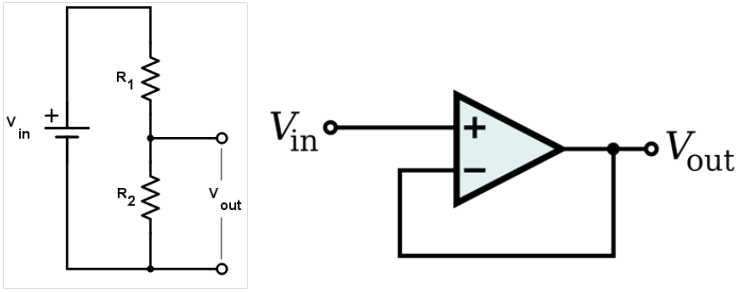

(a) Voltage divider structure

(b) Voltage buffer (or follower) topology with an operational amplifier

Figure 3.7: Voltage divider and voltage buffer schematics

3.2.1.3 Shared sensing

Knowing the final pursued scenario includes many transmitting coils with the same sensing circuit, an idea was to make them share one unique sensing circuit. It would allow having less tracks or wires from the coils to the controller as well as less sensors. Optocouplers would play the role of the switches that would connect and disconnect each coil to the sensors in a determined sequence.

A big disadvantage would come from the coils that were not sensed, since they would not charge as the current sensors the middle of the power flow would interrupt the transmission if disconnected. Another disadvantage is the elevated cost of the optocouplers. Nonetheless, this option appeared to be the fastest way to explore the shared sensing idea, and it could still be improved in future versions.

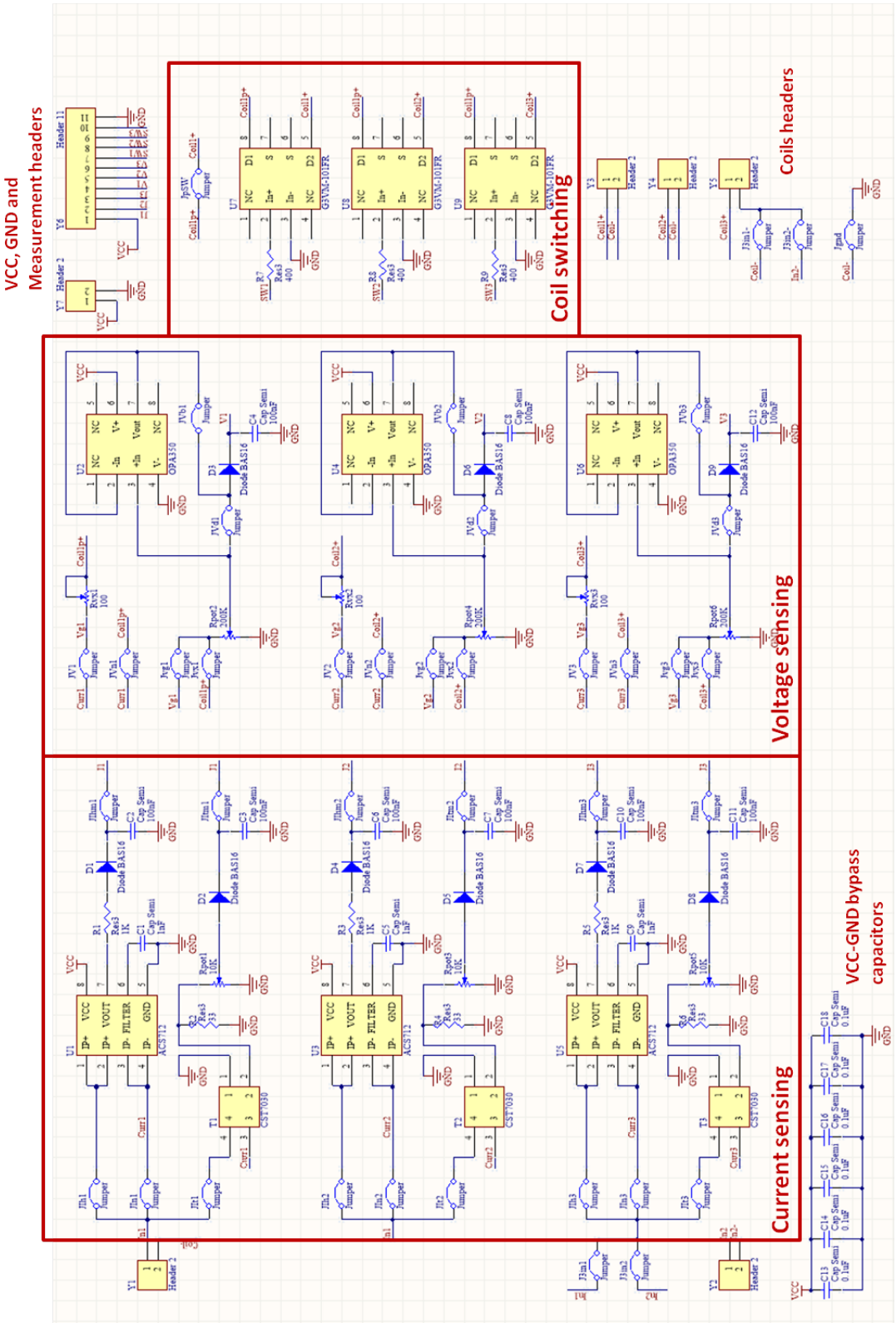

Figure 3.8: PCB v1 Altium schematic with indications of the different parts that compose the circuit

3.2.2 Board evaluation

After the PCB layout was designed and, then, manufactured, it was the turn for the testing stage. The evaluation would be made for, at first, only one of the sensing paths (the three of them were identical), and one sensor at a time (bypassing the rest with jumpers). The tests would start with the application of DC signals to verify the connections and set up the potentiometers. Low power AC signals would be next, before applying the high power 6.78 MHz signal with the amplifier.

In this section, not many quantitative results and plots are shown since the tests were quick and to simply determine which ideas were good, and which parts had to be modified or deleted in the second version.

Current sensors

The first element tested was the Hall effect current sensor. When applying a DC voltage and, having a known resistor as the amplifier's load, the result was close to the expected linear transfer function for the current versus the voltage.

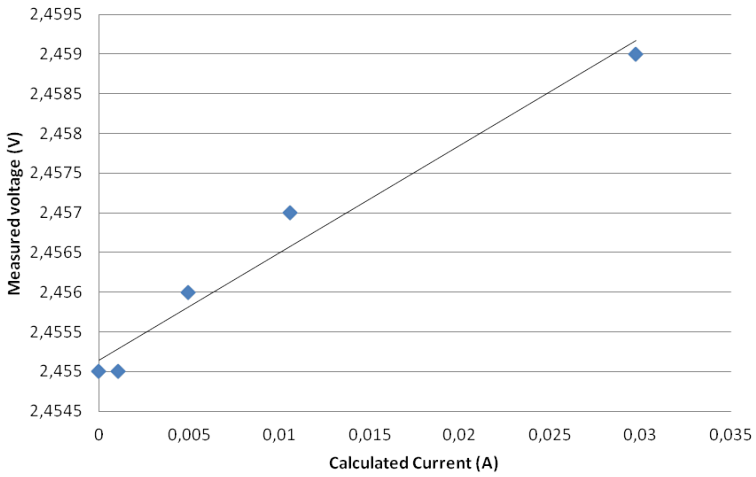

Figure 3.9: Measured voltage versus the calculated current that each measurement represents

At the time when an AC signal was used, and having the transmitting coil as a load for the amplifier, no response was seen on the other side of the receiver. The Hall effect sensor was only reacting to a DC excitation. This option would be rapidly discarded.

When testing the second configuration, the transformer would not show any response for any combination of input signal and load. An error in the implementation on the PCB and the transformer selected were the reason for that. On the other side, the amplifier would not modify its behavior due to the presence of the primary winding of the transformer in the circuit. This option was still the favorite one, with some changes planned towards the second version.

In the last option, the voltage detection before and after a known resistor, the amplifier would not even work properly due to the presence of that resistance in the middle of the

circuit. Option discarded as well.

Voltage sensors

An error with the OPA350's footprint on the board did not allow testing it. However, the simple voltage divider (with adjustable resistors) and rectifier would provide the information without interfering with the circuit. The rectifiers were the worst elements here, since they would show big ripple at the output. They should be improved in the second version, and the acquisition of data should be made by averaging samples.

Shared sensing

The switching scheme would work as it should when using DC voltages. When AC was used, they would not cut the current flow, but only attenuate it. They are not designed for such high frequencies in the same way than the Hall sensors, they perform well only under the 50 Hz from the grid.

The switching approach then, for digital configuration of the current paths, would be more complex and other circuits might be designed.

Overall efficiency

The end-to-end efficiency of the system was evaluated with multimeters measuring the DC currents flowing into the amplifier and coming out from the receiver. The two scenarios, with and without the sensing board in the middle of the power path, were compared.

The voltages were known: 19.5 V was the voltage at which the amplifier was powered (laptop charger), and the receiver's output was 5 V (voltage to charge a phone). With that and the measured currents, the total power efficiency would be easily calculated.

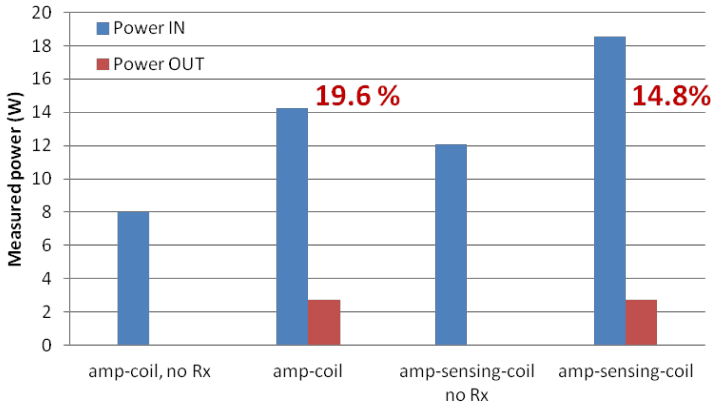

Figure 3.10: System end-to-end power measurements and total efficiency calculation with the sensing PCB v1

The configuration of the system would not be modified for the different measurements. The coils would always be the same, and the distance and relative position of the receiver over the transmitter would not be modified either.

From the measurements, some interesting observations can be made. First, the total efficiency of the system was degraded almost a 5% when the sensing board was used. The result was the same with all the elements bypassed on the board or when making the current flow through the transformer.

Secondly, it can be determined whether there is a receiver charging just by the change of current flowing to the amplifier.

A second observation is that, with these measurements, it is impossible to know at which stages the power was dissipated (amplifier, sensing, transmission or receiver) or what are the parts that modify their efficiency with the presence of the sensing PCB.

Nonetheless, the power transfer would occur when having the sensing board in the system and the received power would still be around the same value.

3.2.3 Observations and lessons learned

- Hall effect current sensors only work properly with very low frequencies. They are designed to detect currents from the grid, at 50 Hz.
- Placing a resistor in the middle of the power flow is not a desirable option since it degrades the amplifier's performance.
- The selected option for current measurement would be the one using a transformer. It would not affect the amplifier's performance and theoretical analysis (and simulations) supported this approach.
- A voltage divider with big adjustable resistors is enough to detect the voltage amplitude and not interfere with the main circuit.
- The rectifiers used were very simple and the waveforms they provided were far from a perfect DC signal as expected. Better rectifiers or sampling techniques such as averaging would be required.
- The optocouplers selected were designed for low frequency AC signals. Other approaches should be explored for the switching action.
- The sensing board degraded the overall performance of the system but not in a critical way. This issue could be solved by working on impedance matching networks at the interface between sensing and amplifier.
- The configuration and elements bypassing with the jumpers on the PCB was a useful solution.
- The connections through jumper wires to amplifier and coils were not reliable. The waveforms would be modified by simply touching or moving those wires. Better connectors were needed.

- The power supplied to the sensing board was 1 Watt, higher than expected. The active components were the Hall sensors, operational amplifiers and optocouplers. This high power consumption was due to the error in the operational amplifier's footprint, that connected VCC to an undesired node.

3.3 Sensing Printed Circuit Board v2

The objective this time was to build this second version to continue improving the sensing elements, but having a more functional sensing board, something that allowed taking some more reliable measurements than before. It would still be configurable so the elements could be tested separately or disconnected if not performing well. Everything learned from the first attempt would be very valuable at the time of deciding the features and design for the second version. The schematic, PCB layout and BOM can be found in Appendix A.2

The main objective remained untouched: to measure current and voltage amplitudes and their phase difference right before the transmitting coil.

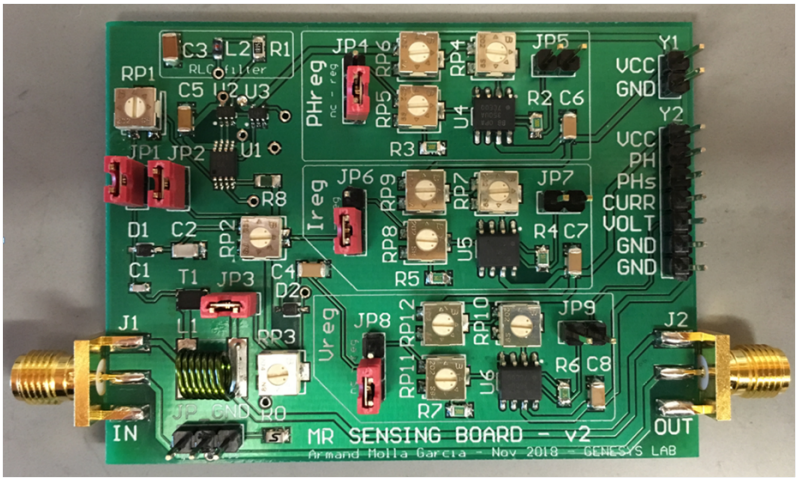

Figure 3.11: Second version of the sensing board, smaller, and for only one coil

3.3.1 Board features and elements design

After all the conclusions and observations explained in Section 3.2.3, some design decisions had to be taken regarding the elements and the features to be included in the second version.

Since the sensing scenario is not simple and it is hard to do several new things right at the same time, it was decided to eliminate several elements from the first version. This would allow making this second board smaller and closer to the basic objectives. Then, other elements would be added, like a first approach for the phase difference calculator. The changes and features that this second board includes are:

- Only one current sensing method, the transformer one. It would be revised and simulated.
- The voltage sensor would simply be the voltage divider. The buffer was not needed.
- Only one amplifier and one transmitting coil would be connected to the board.
- No shared sensing circuits, this issue might be solved in future designs.
- A phase difference detection circuit would be added.
- SubMiniature version A (SMA) RF connectors for both amplifier and coil to avoid noise and fluctuations due to the connections.
- More ground pins for easier testing
- Jumpers to connect or bypass sections of the circuit
- Circuits to adjust the value and span of the voltages read by the Arduino would be included.
- The rectifiers would still be implemented with the simple structure of diode plus capcitor, but better Shottcky diodes would be used (RB751V40T1G by OnSemiconductor) [20].

This time, all the elements on the board, except for the voltage divider to detect the voltage amplitude, were simulated using Cadence.

3.3.1.1 Current sensing through a transformer

After failing the first attempt of implementing the current sensor with the transformer, but knowing that this was an approach that could work, the design was revised and other implementations were searched in the literature. Finally, a design proposed in [14] was simulated and used, this time with a 1:1 PFD3215 transformer [21].

The current measured would be the one flowing through a power inductor inserted in series with the amplifier (I_{sens}), which performs as the current sensor. Then, the transformer would act as an insulator, being connected in parallel with the sensing inductor. This new configuration provides lower sensor's equivalent impedance, hence, better connection between amplifier and transmitting coil. In the first approach, these functions were both responsibility of the transformer's primary winding. Another improvement here is the addition of a parallel capacitor (C_{reso}) resonating with the secondary winding's leakage inductance, to convert the current into a large voltage which can be easily rectified. See Figure 3.12a for the described circuit's schematic.

Regarding the simulation, different loads seen by the transmitter would provoke the flow of different currents that would be detected. Using a parametric analysis for the load resistance ($R6$ in the schematic), different current values would be detected. The output

of the sensor is the differential voltage between the nodes of $C2$ (Vm+ and Vm- in the schematic).

Note that the two sides of the transformer would be isolated in the real circuit but, to avoid simulation errors, the same ground node has to be used on both sides. To simulate a scenario close to the real one, a very big resistor is placed between Vm- and ground. To avoid confusions or differences with the fabricated circuit, the "Ground test jumper" is added to the design, to be able to play with different possibilities of ground isolation. See Figure 3.22 for the complete schematic and its parts.

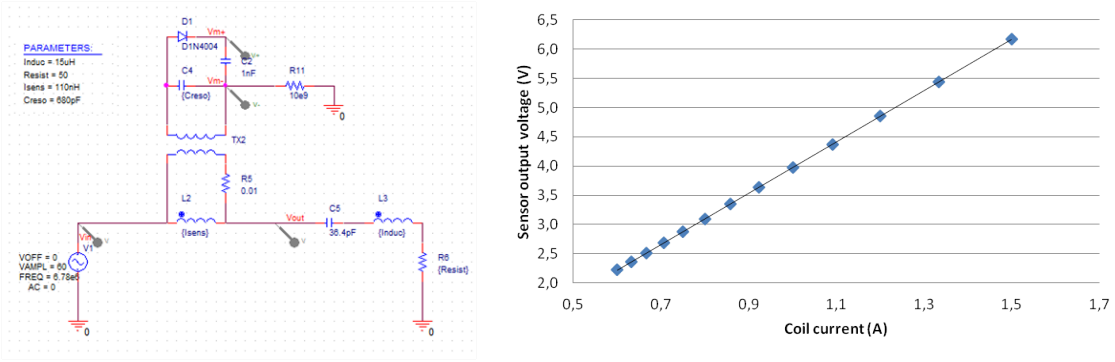

(a) Transformer sensor circuit schematic

(b) Current sensor transfer function

Figure 3.12: Transformer-based current sensor schematic and simulation results

The results show the sensor should perform as desired, providing a linear response with every 1 V at the output corresponding to, approximately, a 0.2 A current variation in the transmitting coil. This DC voltage proportional to the AC current flowing to the coil is the exact aimed behavior, as already theoretically demonstrated with the equations in Section 3.2.1.1.

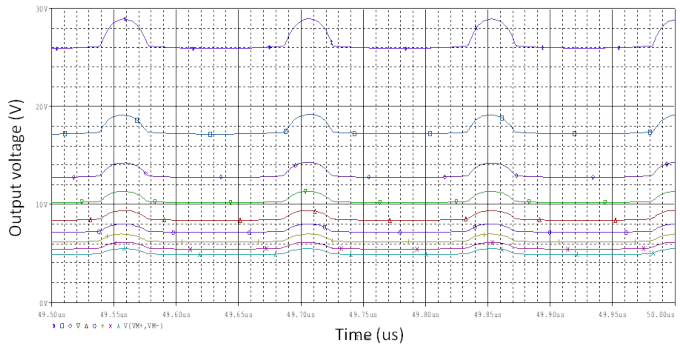

Figure 3.13: Current sensor's output voltage versus time for different arbitrary current values.

Something found in the simulations was a small ripple on the output voltage at the carrier frequency of 6.78 MHz. However, this issue can be easily solved by averaging measurements, since those peaks still allow the output voltage to be very uniform. Figure 3.13 shows the simulated output DC voltages obtained for different load values with this undesired ripple. Note that this plot is important for the appreciation of the output voltages' waveforms, not for their trend. The different plotted voltages correspond to

several provoked currents, which do not necessarily have to be equally spaced. Figure 3.12b already showed the linear trend of the sensor's transfer function.

The same results were obtained when the 1 GΩ resistor solution was used on the other side of the transformer.

3.3.1.2 Phase difference detector

The phase difference detector might have several possibilities to be implemented, but the solution chosen was also taken from an idea provided in [14].

With the use of comparators between the signals of interest and their own ground, square signals with the frequency information would be generated. Then, the time interval between rising (or falling) edges of each signal is the phase difference between current and voltage. This phase difference would be outputted in a Pulse Width Modulation (PWM) format after comparing the signals through an XOR gate. Determining the sign of the phase would be done with a flip-flop. The schematic can be seen in Figure 3.14. Note the inclusion of the current and voltage sensors as well in the schematic, since they are required to allow the phase calculation.

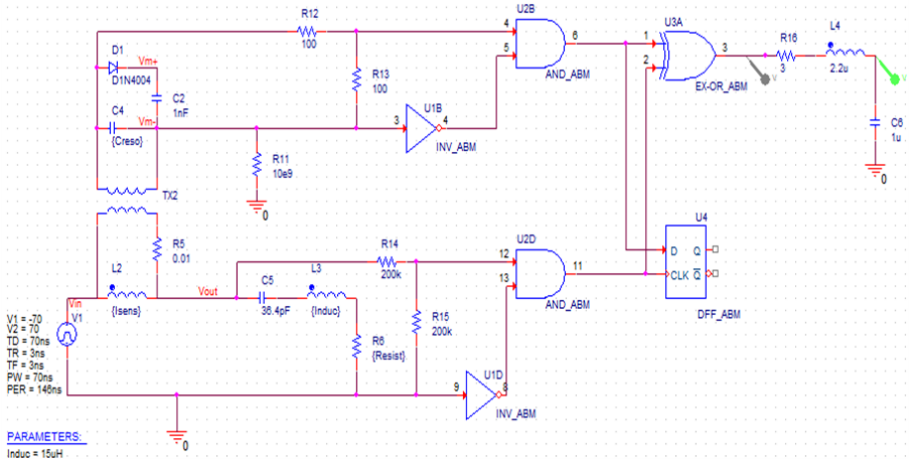

Figure 3.14: Full phase detection simulation schematic

Note that, the comparators that would be used in the real design, were implemented by means of AND gates and an inverted input with a NOT gate in the simulation schematic. The behavior is equivalent.

Taking a look at the signals after the comparators and the sign and magnitude outputs, it was verified that the proposed design worked as predicted, at least, in the simulation environment.

From the plot in Figure 3.15a, the observation to be made is that, as expected, the two signals have a certain phase difference and the comparators job of keeping this information with digital signals is accomplished. One of the signals has a different rising and falling time due to the difference in the two signals before the comparator. The Red trace carries the voltage information, which is taken through a voltage divider and comes directly from

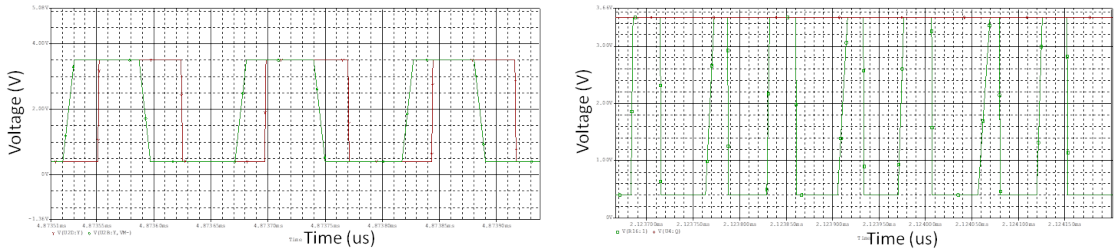

(a) Square signals with frequency and phase information for current and voltage

(b) Magnitude PWM output and sign binary otuput

Figure 3.15: Digital signals after the comparators and after the flip-flop and XOR gate.

the source, it is a neater signal. On the other side, the current information is carried by a voltage which has gone through the transformer stage, where the signal is distorted a bit.

In Figure 3.15b, the outputs for the sign and the magnitude are shown. The sign binary output has no complication, it is always high here since the current is leading the voltage. The magnitude PWM has double frequency (13.56 MHz) after the XOR gate as expected since it is high every time the voltage and current square signals are different. The only anomaly observed here is the slightly different pulse widths, which come from the difference in the rising and falling times. After the filtering stage though, these differences would not be relevant and the different phases would be detected.

Finally, an element that had to be simulated and calculated separately was the output filter. In order to get a DC voltage out of the PWM signal, a low pass filter was the option chosen. This filter would keep the DC component and eliminate the rest of the harmonics of the square signal. A second order filter would perform good enough for the detection, and an automatic calculator was used to determine the RLC values. The schematic and simulation results for different pulse length can be appreciated in Figure 3.16.

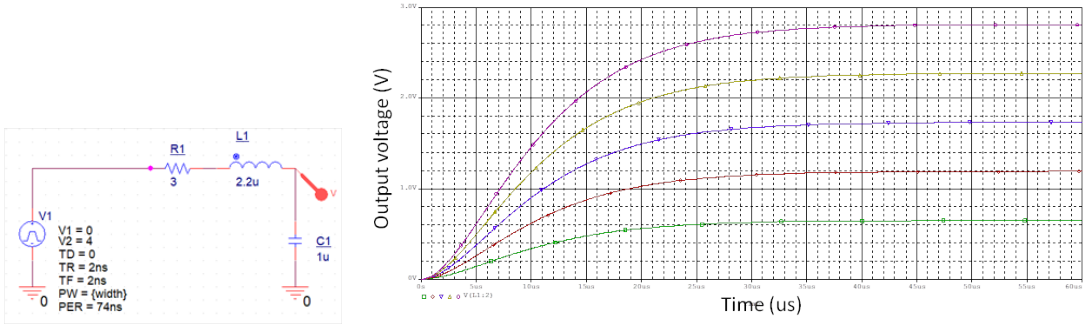

(a) Chosen second order RLC filter schematic

(b) Filter output voltage versus time to observe the overshot and settling time

Figure 3.16: Second order RLC filter schematic and time domain response

After experimenting with several options, a high cut-off frequency of 30 kHz was selected as it would be enough for our design. That lead to a settling time of about 40 microseconds as seen in the simulation results from the previous figure. The reason for this decision was obtaining close to commercial values for the components, and having capacitor and coil values that could be found in small surface mount encapsulations.

When using the designed filter at the output of the complete phase detector circuit, the response was favourable again, with a small ripple of around 80 mV. The magnified output signal with the ripple can be observed in Figure 3.17b. Here again, averaging a reasonable amount of samples would give consistent results.

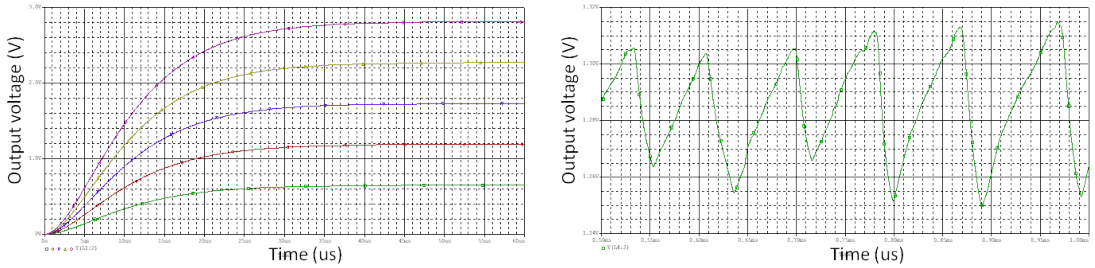

(a) Phase magnitude output voltage (b) Output voltage ripple

Figure 3.17: Phase detector magnitude output and ripple appreciation from the full circuit simulation

Finally, the transfer function of the phase difference magnitude detection could be plotted, showing a very nice and linear behavior as desired.

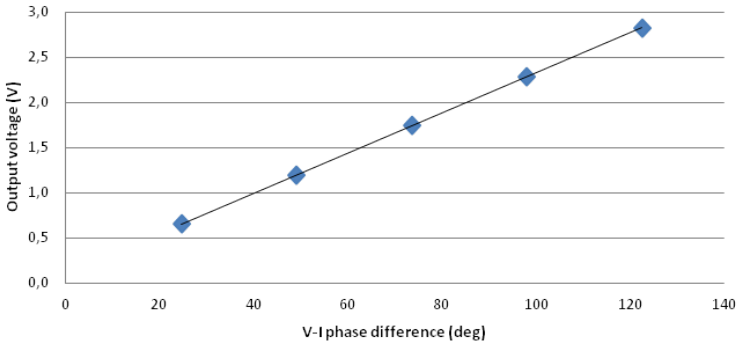

Figure 3.18: Output phase difference magnitude voltage versus voltage to current phase difference

3.3.1.3 Voltage range adjustment

An additional stage included in this second version of the sensing circuit is a voltage conditioning structure. In the the best case scenario, the output signals for current, voltage, and phase information would be voltages ranging from 0 to 5 Volts, to take advantage of the whole range of the reading Analog to Digital Converter (ADC). In reality though, it is not the case.

After the simulations and observations of the behavior of the amplifier and coil, the changes we want to measure tend to be small, thus, the voltage variations at the sensors' outputs are not as big as 5 V. For that reason, the presented circuit allowed scaling those output signals for better reading. Three identical circuits would be used, one for each sensor.

The schematic used for the simulations is presented in Figure 3.20. In the PCB design schematic from Figure 3.22, some resistors appear as potentiometers, which would allow the adjustment of the voltage levels after observing the real voltages provided by each sensor. This scaling action is implemented with an operational amplifier configured with the differential amplifier topology.

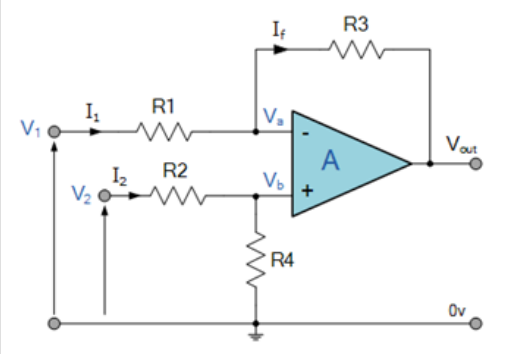

Figure 3.19: Differential amplifier topology used. The components' names can be identified in the gain equation

The equation that relates the resistors in Figure 3.19 is:

$$V_{out} = -V_1 \left(\frac{R_3}{R_1}\right) + V_2 \left(\frac{R_4}{r_2 + R_4}\right) \left(\frac{R_1 + R_3}{R_1}\right) \tag{3.11}$$

where, if R1 = R2 and R3 = R4, then:

$$V_{out} = \frac{R_3}{R_1} (V_2 - V_1) \tag{3.12}$$

The scaling action is composed by two steps: firstly, the sensor's output voltage is compared to a DC reference to get rid of the offset. This is done by connecting a voltage divider from VCC (5 Volts) to the inverting input of the amplifier to make V2 in the schematic be a fixed voltage. Secondly, the amplifier magnifies or reduces that voltage level to make the maximum voltage gathered from the sensor be as close as possible to 5 V. The voltage divider ratio and the gain (Equations 3.11 and 3.12) would be adjusted with the mentioned potentiometers in the final design. R1 and R2 would adjust the gain, and an additional potentiometer would determine the voltage V2.

The simulations were made using the phase detector output filter as the input for the amplifier since it would be one of the real cases. Figure 3.21 shows the difference between the range of voltages at the input and output of the amplifier.

Observe, in the plots from Figure 3.21, that the input voltages range from 0.65 to 2.8 V and, for a specific voltage reference and gain, the output's range becames 0.25 to 4.8 V, which is almost the complete input range of the ADCs. The simulation results verified the theoretical study.

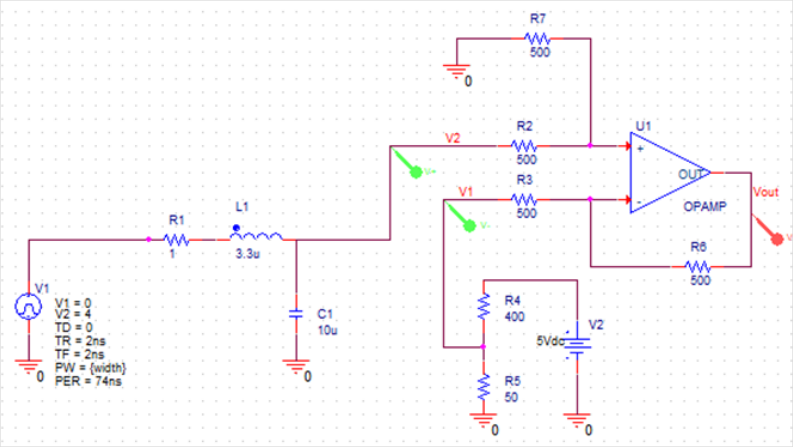

Figure 3.20: Differential amplifier-based voltage regulator. Here, after the filter used in the phase detector

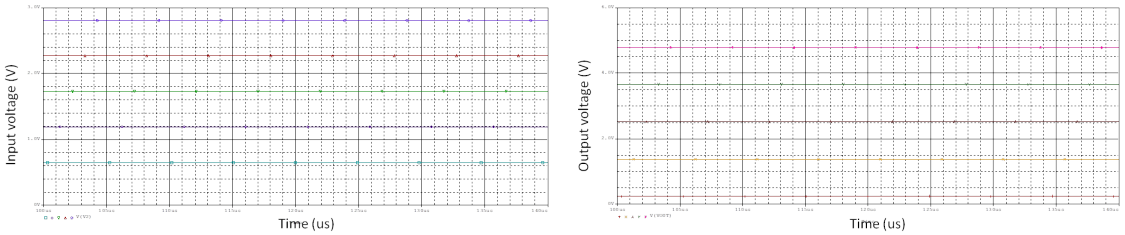

(a) Input voltages before being scaled

(b) Scaled output voltages.

Figure 3.21: Simulation results for the differential amplifier scaling circuit at the input and output

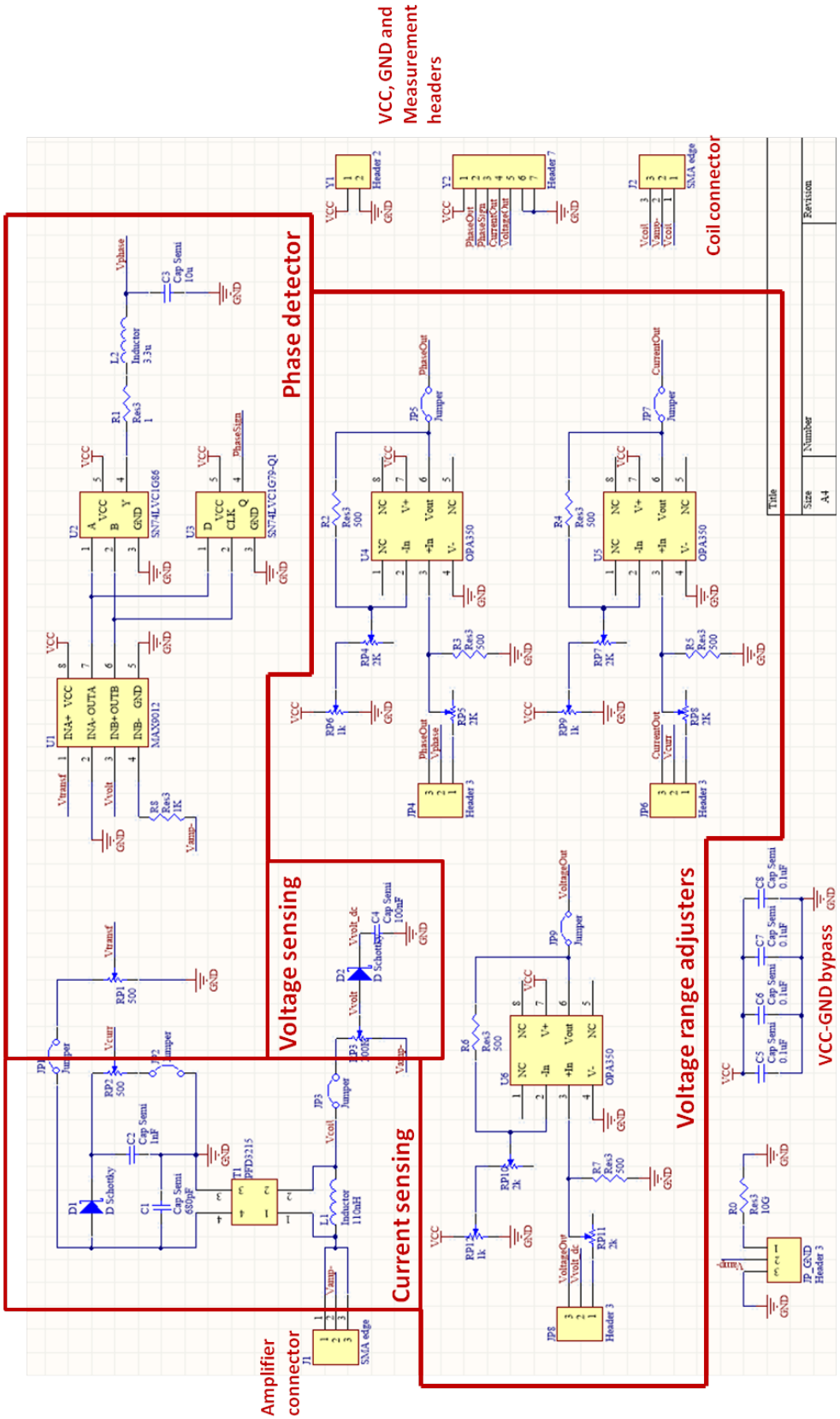

Figure 3.22: PCB v2 Altium schematic with indications for each of the different parts that compose the circuit

3.3.2 Tests and results

The way of connecting this sensing board can be seen in Figure 3.23, in between the amplifier and the transmitting coil. The SMA connectors made it easier and more compact this time.

The tests that required a receiver were performed with an EPC 10 W receiver connectec to a litium-ion battery through its charger as the receiving load . See Figure 3.24.

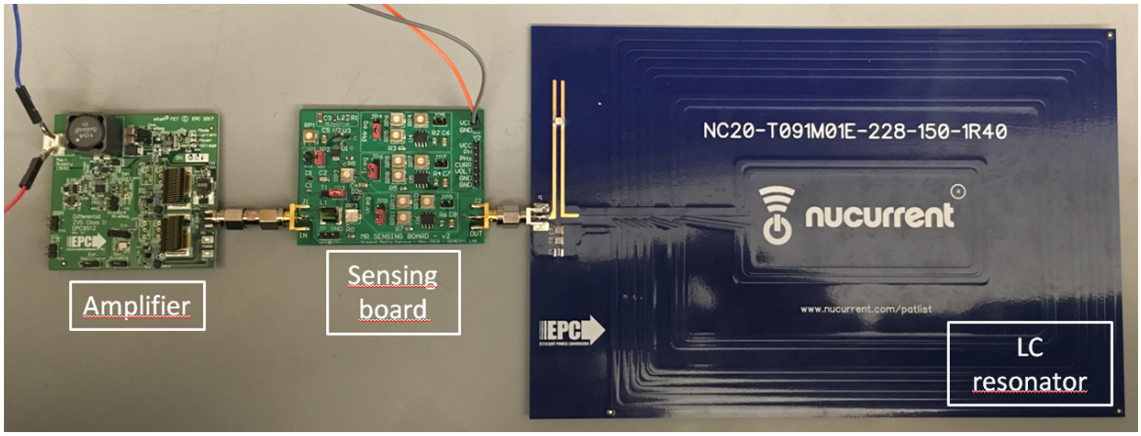

Figure 3.23: Amplifier, Sensing PCB v2, Transmitting resonator setup

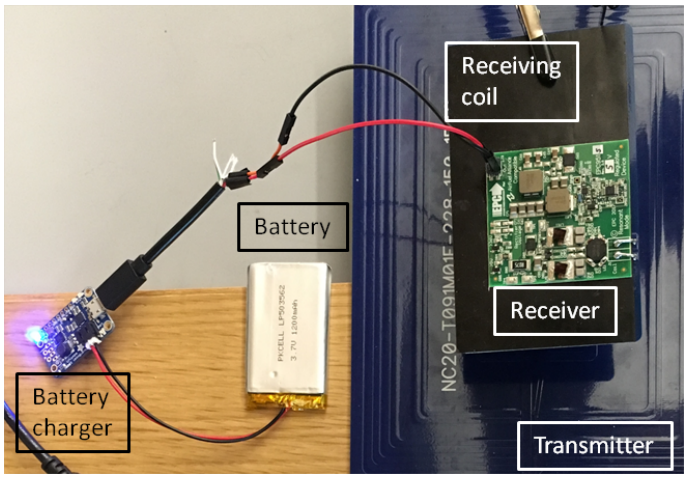

Figure 3.24: Test receiver structure

3.3.2.1 Input-Output comparison

One of the problems found with the fist version of the sensing board, was the distortion it added to the power signal. The connections and routing on the board were improved in this second version to improve this characteristic. The impedance matching would also play a role here, but it was left as an improvement for a future version. Ideally, the power signal should get to the transmitting coil unmodified after travelling through the sensing board. Additionally, it should be as close as possible to the signal observed when

the sensing board is not used and the amplifier is directly connected to the coil (as it is designed and supposed to be used). The following measurements were made without the presence of any receiver.

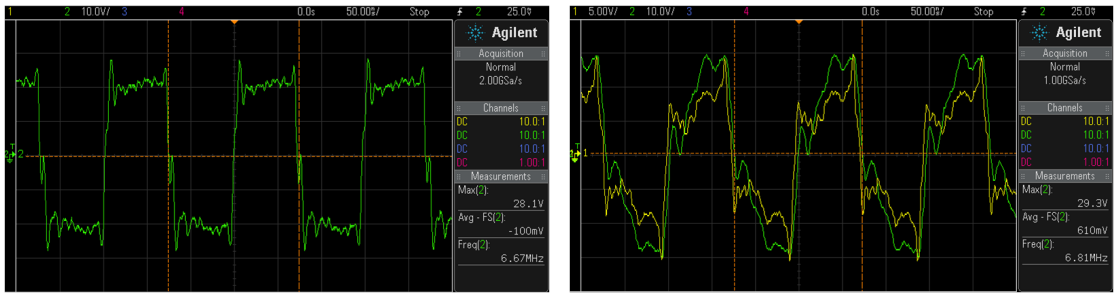

(a) Best case power waveform provided by the amplifier

(b) Input (yellow) and output (green) waveforms for the sensing board

Figure 3.25: Power transfer waveform observations with the oscilloscope

Figure 3.25a shows the aspect of the square wave provided by the amplifier when it is directly connected to the transmitting coil. Figure 3.25b shows how this waveform is distorted when the sensing board is used. The signal still resembles a square signal but much less perfect. It is positive that input and output are not very different from each other.

From this, two observations can be made: the board does not modify the signal it gets at the input (more than small differences), and an impedance matching network might be needed in order to make the total load be in the range that allows the amplifier to provide the best square wave possible. Apart from this issue, when the receiver was placed over the transmitter, it would charge.

3.3.2.2 Voltage regulators

The voltage regulators (described in Section 3.3.1.3) performance was quickly tested with the use of DC signals. The connections were verified to be correct and the expected behavior was observed.

The experiment case consisted of giving as an input of 6 V while the inverting amplifier input reference was set to 4 V and the gain equaled 1. The voltage obtained at the output, as it had to be, was $(6 - 4) * 1 = 2V$.

3.3.2.3 Current sensor

To evaluate the current sensor performance, the oscilloscope probes were connected to the output of the transformer and after the rectification of the previous signal. The first measurement would directly show the voltage signal proportional to the input current, the second measurement would be the extracted DC level with the current amplitude information.

Making reference to the names in the schematic in Figure 3.22, the first case corresponds to the fourth terminal of the transformer T1 and, the the second case, to the node

named Vcurr (the third terminal of potentiometer RP2, which acts as a voltage divider).

(a) Induced voltage on the secondary winding of the current sensing transformer

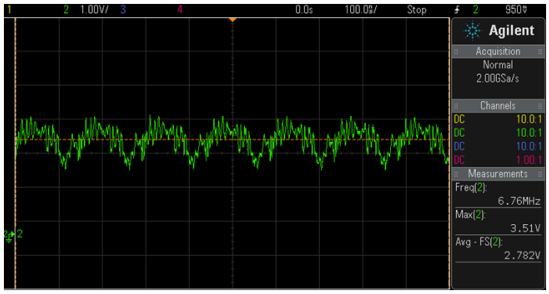

(b) Rectified voltage after being scaled through a voltage divider

Figure 3.26: Current sensing circuit oscilloscope measurements without receiver

Figure 3.26a shows the aspect of the time signal measured after the voltage is induced on the transformer's secondary winding. Taking into account the input signal seen in Figure 3.25b, the obtained response is adequate. It is clearly an AC signal at the transmission frequency with an amplitude of 9.4 V. In Figure 3.26b, the scaled down and rectified voltage can be seen. The ripple is evident, however, it has a clear DC component. The oscilloscope's screen averaging shows a value of 2.8 V. This same averaging would be performed after the MCU's measurements.

The same two signals were observed when the receiver was placed over the transmitter.

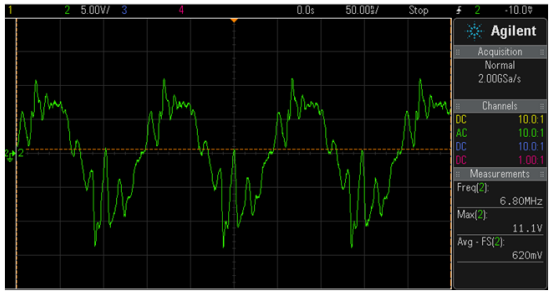

(a) Induced voltage on the secondary winding of the current sensing transformer

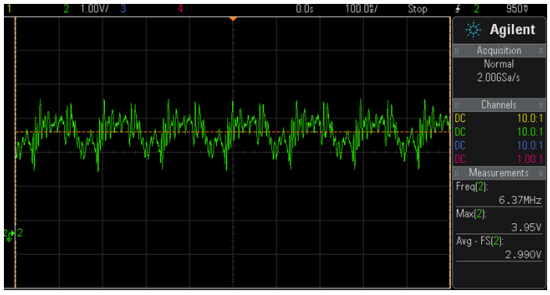

(b) Rectified voltage after being scaled through a voltage divider

Figure 3.27: Current sensing circuit oscilloscope measurements while charging a receiver

Here, very similar results were obtained, however, two main differences can be appreciated: the receiver would produce an amplitude increase and the signal would become more noisy. The amplitude change verifies the fact of the proportionality between current through the primary winding and the induced voltage. Since the receiver presence provoked an increase of the current flow, the observed voltage amplitude raised to 11.1 V. The noisier signal is due to the change of impedance (load) that the receiver's coil produces. The transmitter sees an even further away from optimal load and its output signal gets worse. The rectified voltage is noisier as well, but its DC continues giving the desired information being, this time, 3 V.

Summarizing, the current sensor at its output,after rectification and scaling the voltage down through a voltage divider, offered an averages difference of 0.2 V when a receiver

was charging. Then, there would still be some room for improvement using the differential amplifier to get an even broader difference. Figure 3.28 exemplifies the trade-off observed when using the regulation part: the more amplification needed, the more noise and signal amplitude.

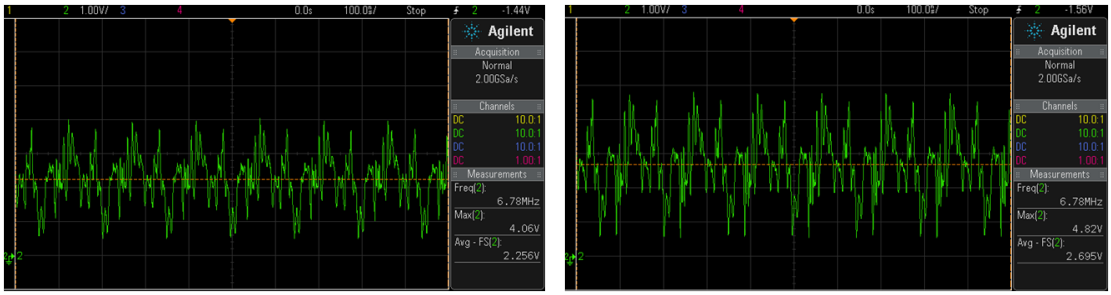

(a) Current sensor regulated output voltage with no receiver

(b) Current sensor regulated output voltage with receiver

Figure 3.28: Second board's current amplitude measurement output with its regulation phase active

In order not to cut the signal low peaks and not affect the averaging, the voltage difference could not be amplified to several volts. Here, the voltage reference and gain were set to 1.1 V and 2 respectively. The voltage difference between averages became 0.45 V, from 2.25 V without receiver to 2.7 V when a receiver was charging.

With the full current sensing block working and the possibility of detecting whether a receiver was placed over the transmitter, an Arduino Mega was connected to the PCB to gather this data.

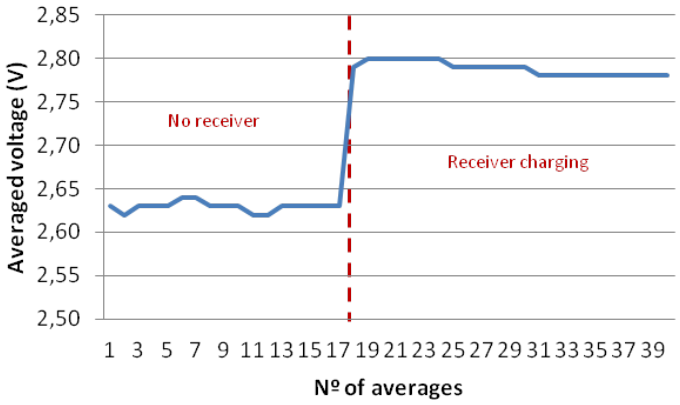

Figure 3.29: Averaged measured voltage versus time for current measurement with an Arduino

The result was similar to the previously described, nonetheless, the voltage average difference captured was never more than 0.2 V. This might have been due to the Arduino's sampling frequency, by far not high enough to take as many samples as the oscilloscope.

On the bright side, an appealing feature observed when measuring was the low variance of the obtained value. The averaged voltage would have a ripple of only ± 0.01 V. This way, even though the averages difference was only 0.2 V, the step change would be clearly

detected by the MCU. Figure 3.29 shows a plot of the measured voltage versus averages (time) with the two scenarios.The Arduino code for this measurement can be found in Appendix A.3.

Another interesting behavior was observed when the receiver was left charging for longer time over the transmitter. The measured voltage would slowly drop, which indicated battery charging. When the receiver's battery level was lower, less current would be demanded, and that could be monitored through the designed measurement circuit. Figure 3.30 is a plot for two different distances between transmitting and receiving coils where this slow voltage decay can be appreciated.

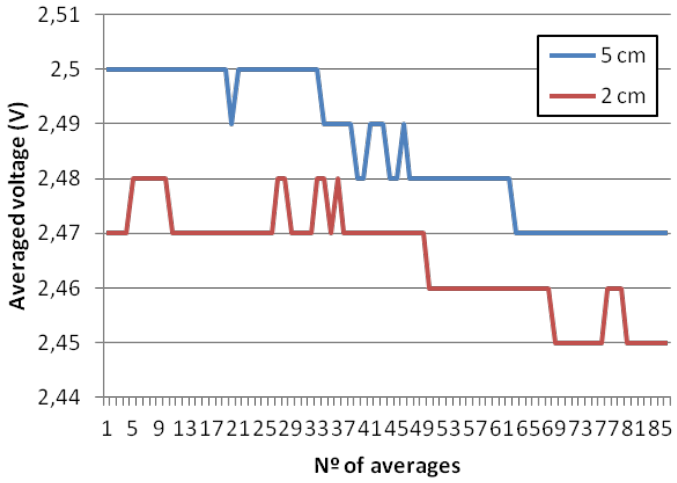

Figure 3.30: Current sensor averaged measured voltage versus time for two different distances between transmitter and receiver

Additionally, a voltage level observation can be made. Here, the closer configuration demanded less current than the situation with 5 cm of separation. Interestingly, the voltage at the beginning of the 2 cm experiment is the same as the final voltage for the 5 cm one. This happened because the 2 cm case was tested right after the first one and the battery level continued charging from the same point. It verifies the dropping characteristic of the charging but, at the same time, tells that the charging distance cannot be estimated using the current measurement. The amplifier tries to keep charging at the same rate regardless of the distance.

3.3.2.4 Voltage sensor

The voltage sensor, as in the first sensing board design, consists of a simple voltage scaling through a voltage divider, a rectifier and the reading from the MCU.

First, the signals observed with the oscilloscope on the board were the ones shown in Figure 3.31.

The rectification, again, was made by a very simple rectifier. Considerable ripple would be present in the ideally DC signal. The regulation phase follows exactly the same

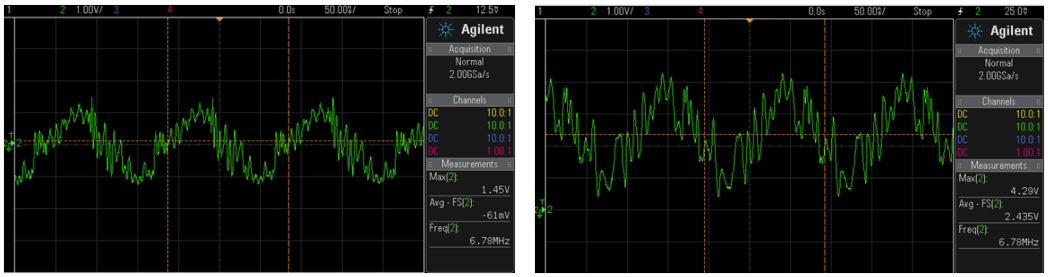

(a) Sensed voltage signal after being scaled down by a voltage divider

(b) Voltage measured by the MCU after rectification and regulation stages

Figure 3.31: Voltage sensing oscilloscope voltage measurements

structure as for the current measurement. This time, the voltage reference was set to 1.2 V and the gain of the amplifier would be 1.4. This is the reason why the rectified peak to peak voltage is even bigger, but always between 0 and 5 Volts. However, in the same way as for the current measurements, there was an evident DC component that would be detected by averaging samples of the signal.

An Arduino was used again for the averaging (1000 samples) and measurements digitization. The presence or absence of receiver scenarios would be compared.

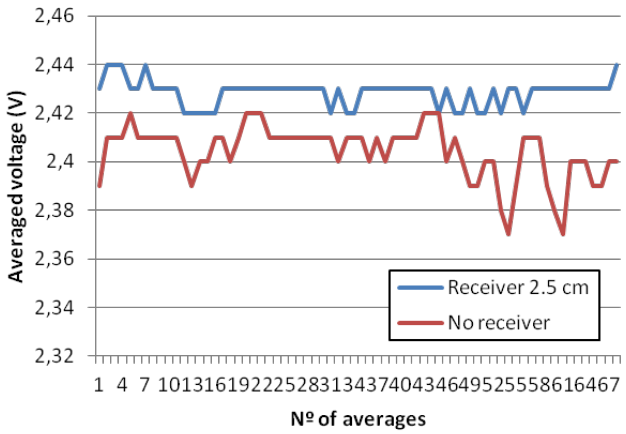

Figure 3.32: Voltage sensor averaged measured voltage versus time with and without receiver charging

There is a slight difference between the two scenarios but not enough to state we can take the decision looking at the voltage difference. The amplifier responds differently with and without receiver, but it tries to keep the voltage constant.

This measurement would be useful not to make precise detection of receiver presence or distance of charging, but for system failure or misappropriate performance.

3.3.2.5 Phase detector

Making reference to the components seen in Figure 3.22, the phase detection circuit starts comparing the voltages coming from the voltage dividers implemented with RP1 and RP3.

When testing with the signals coming from the amplifier, the behavior was not the expected. The input signals to the phase detector would be noisy, so the comparators would not be able to provide neat square signals at their outputs. Figure 3.33 shows the signals at the comparators' inputs and Figure 3.34 at their outputs.

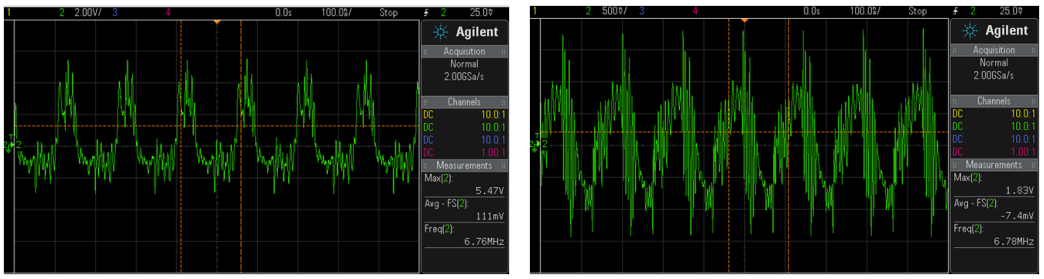

(a) Input signal coming from RP1 (b) Input signal coming from RP3

Figure 3.33: Phase detector input signals observed on the oscilloscope

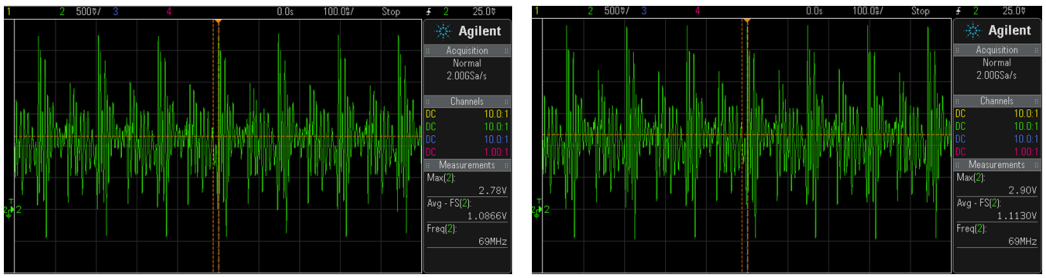

(a) Current phase information carrying signal (b) Voltage phase information carrying signal

Figure 3.34: Phase detector comparators' outputs

It can be observed how the input signals were not close to square signals and had a noisy nature. After going through the comparators, the results were even worse. Those signals could not be useful and it made no sense to analyze how the following components would respond.

When the comparators were tested separately using DC signals, they would work as expected when high or low voltages were applied. They were not the origin of the problem. Better signal conditioning and filtering are needed to properly implement a phase detector in this scenario.

3.3.2.6 Efficiency evaluation

The last figure of merit to be measured was the efficiency change when the new sensing board was introduced in the circuit.

The efficiency results would be found in the same way as for the first version PCB, calculating the end-to-end efficiency by means of multimeters measuring the input and output DC currents flowing to the amplifier and from the receiver. The standard case without any sensing, and the cases with each of the sensing boards designed in this thesis are compared. The receiver would always be placed in the same position and distance for the charging situations.

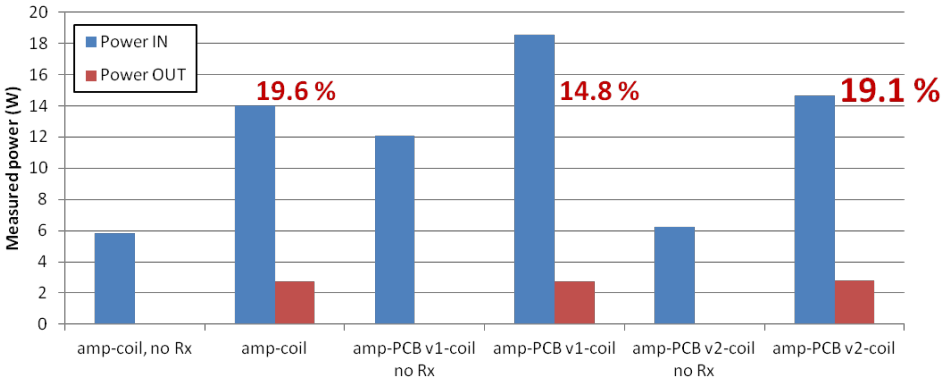

Figure 3.35: Measured input and output powers and end-to-end efficiency

Figure 3.35 compares all the possible scenarios. In the first place, comparing the three configurations without a receiver charging, it is clear that the first sensing board produced an unreasonable increase of the consumed power. It was, mainly, due to the connections and the power tracks on the sensing board. For the second version, where the connections were implemented using SMA connectors, and the power tracks on the PCB were of equal length and without many elements connected to them, a clear improvement can be seen. This second sensing board only increases the consumed power by 0.4 W, while the first one supposed 6.2 extra Watts.

When comparing the performance at the output of the charging receiver, a similar situation takes place. While the first sensing board increased a lot the input power, and the total efficiency dropped almost 5%, the input power increase is very low, and the efficiency drop is reduced to achieve a 19.1% end-to-end efficiency.

The sensing PCB v2 means a clear improvement for this issue detected with the first sensing solution. The better connectors and power paths without obstacles achieve reducing the load variation seen by the transmitting amplifier.

With the use of impedance matching networks and transmission line analysis in future versions, very close values to the case without sensing could be reached.

3.3.3 Conclusions and future work

The sensing board evolution has been favourable as verified in the testing section for the second version. The objectives of sensing voltage and current have been achieved even though not with the ability of knowing their real values with good precision. Other objectives have been achieved and some features were left for future improvements in the sensing block. The phase difference detection has been designed and simulated, but the real tests have showed some more difficulties are to be overcome to get the desired results.

The following list summarizes the main features achieved after the whole sensing block development process:

- A sensing board that provides information about the power signal, and is placed

in the power path to the transmitting coil has been successfully designed while not influencing negatively the charging action.

- The current sensor allows detecting the presence of a receiver charging over the transmitting coil. It also allows detecting the charging rate as the current detected drops.
- The current and voltage sensor architectures are completely passive, thus, they do not need power supply, which can be easily integrated next to any transmitting coil in different application cases.
- The voltage sensor was successfully built and it can provide information about system failure or malfunction.
- The improved connections make the efficiency drop with respect to the basic case (without sensing) be very small.
- Adequate circuit configurations were used to set the voltages within specific voltage ranges so a MCU could properly read the signals.

On the other side, some elements would still not work as desired or better performance would be preferred. Possible improvements and future steps towards a third version of the sensing board are listed below:

- The current sensor would not allow knowing the real AC current magnitude value due to the lack of calibrated load tests. Fixed calibrated impedance tests would help finding these result.
- The charging rate detection with the current sensor could be better characterized to identify different batteries or other sorts of system failures.
- The rectifiers used were very simple and there was always ripple in the measurements. Reducing this ripple would allow better adjustment of the voltage ranges and more detection sensitivity.
- The phase detector has undergone a first stage of its development, but further work is required in order to be able to get neat and smooth signals before the logic actions take place.
- With the phase information, real power flowing to the transmitting coil would be calculated and, together with the current sensor, impedance variations might be monitored. That would help in, for example, detecting the receiver's dimensions or distance to the transmitter.
- The waveform coming from the amplifier is far from a smooth square signal and there is still a small efficiency drop. Impedance matching and transmission lines analysis should be performed in order to keep the total impedance of the sensing block plus coil be in the specified range by the amplifier's manufacturer.

Lessons learned

Simplification has been one of the main ideas that has helped after the failure of several parts in the first version of the board. For the second version, a simpler, smaller, with less elements circuit was decided to be implemented to focus only on basic aspects to be achieved. It allowed better characterization and understanding through simulations and the results have been favourable.

Another interesting fact has been the production of these two versions one right after the other and in a short period of time, making the author of this thesis go through the complete process of finding a problem, designing a solution, building it, and testing to start the entire process again.

Chapter 4

Variable Load Switching Amplifier

This chapter talks about the amplifier needed to drive transmitting coils in MR WPT systems. Following the charging surface application described at the beginning of Chapter 3, the amplifiers required are another key element for the system.

The first reason the amplifiers are important is the cost, system scalability and efficiency. Ideally, each transmitting coil would need its own transmitting power amplifier for better control and to make sure there will always be enough power capacity to charge all the devices placed over the surface. Then, these amplifiers, the simpler they are, the easier it is to have many of them at lower cost and in a reduced space.

Another advantage of having individual amplifiers for each coil is the possibility of implementing a special kind of BF. This technique, described in the Chapter 5, would allow better coverage of the areas in between transmitting coils, where the charging action becomes harder. It would allow building a surface with fewer coils for charging devices at almost the same rate in any location.

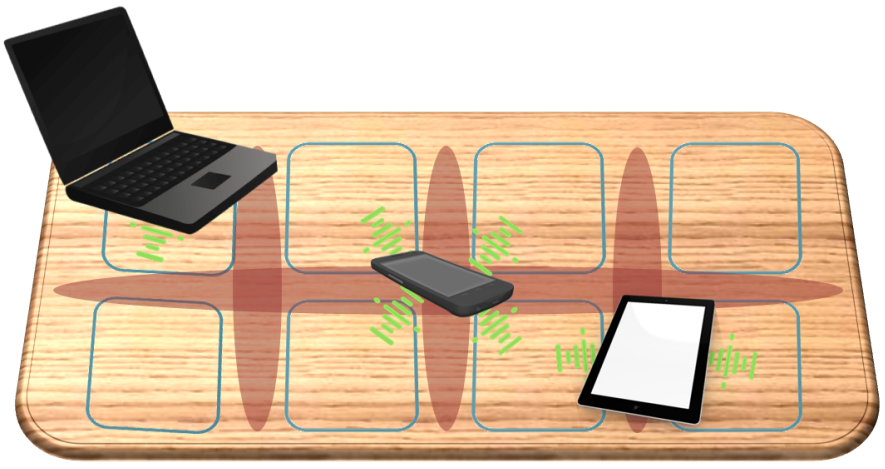

Figure 4.1: Charging surface scenario with the receivers' influence on the transmitters (green waves) and the areas where it is more difficult to charge (red regions).

Then, the variable load characteristic is an important feature to be included as the aimed application would charge multiple receivers at the same time. The transmitters

would experience a load effect produced by one or several devices at the same time. Even in the single receiver case, if different devices such as a smart watch, laptop, phone, lamp or monitor are to be charged, they all have different requirements, thus, their receiving coils are going to be different, what would suppose a different impedance for each of them.

In many situations in Chapter 3, the load effect on the amplifier was what changed the behavior or did not allow to have the desired signals. For this reason, the used amplifier should be able to offer a good performance along a range of loads as broad as possible while maintaining reasonable operating efficiency. The applications described in the following chapters also recall the influence of the varying load effect.

4.1 Amplifier basics and typologies

What we are calling power amplifier is, in fact, an inverter. Its main function is to convert a DC power input into an output AC signal at the required transmission frequency (6.78 MHz in our case) with, ideally, the same power. For practical reasons, whenever we test with a power supply or connect the amplifier through an adapter to the 50Hz power outlet, this input power is always going to be DC. Two inputs are required then, the DC signal bringing the power, and an AC control signal at the system frequency. It can also be seen as a device that adds power to an existing AC signal, reason why they are called amplifiers [22].

Regarding their implementation, there exist several well defined topologies depending on the circuit design. Class A, B, AB and C amplifiers' circuits are the ones called analog designs. The difference between each of them is the proportion of each input cycle during which an amplifying device (transistors usually) passes current. This proportion is called the conduction angle. If the device is always on, the conducting angle is 360°. If it is on for only half of each cycle, the angle is 180°.

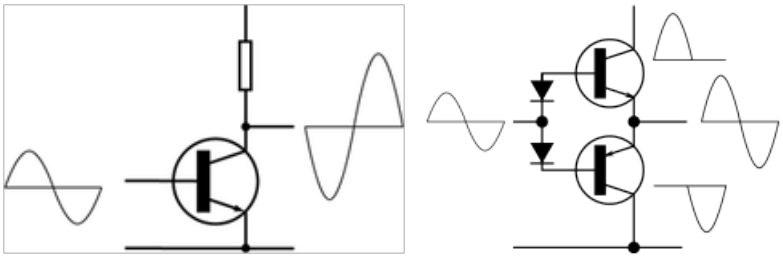

(a) Class A amplifier with a conduction angle of 360º

(b) Class AB amplifier with a conduction angle of slightly more than 180º

Figure 4.2: Class A and class AB amplifiers simplified schemes and the conduction angle concept [2]

The main drawback these amplifiers have is that they suffer from distortion and limited theoretical efficiencies . Class A amplifiers have a conducting angle of 360º and are linear, but their efficiency can never be higher than 50%. Class AB amplifier has a good compromise between linearity and efficiency, but it can never surpass an ideal 78%. Then,

in real scenarios, efficiencies are even lower.

This efficiency limitation the analog designs experience is the reason why the switching designs are of interest here as our application is directly related to power transmission.

Switching amplifiers rely on the use of transistors as switches to generate the desired signal. Here, they would be either completely on or completely off, they do not work in the linear region as in the analog designs. It is the case of class D and class E amplifiers. The amplifying device of choice for this function is, usually, the Metal-Oxide-Semiconductor Field-Effect Transistor (MOSFET) or, more recently, the Gallium Nitride (GaN) Field-Effect Transistor (FET), which offers a faster response and better switching characteristics.

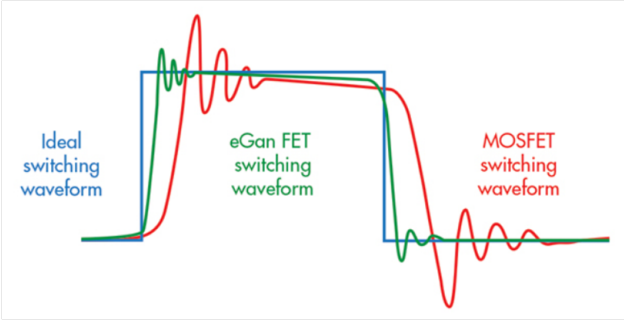

Figure 4.3: Ideal switching waveform versus MOSFET and GaN FET responses [3].

This switching characteristic allows transferring, ideally, up to the 100% of the input power. Their real efficiency cannot be much more than 95% due to the fact that the MOSFETs or GaN FETs are not ideal switches and have some ON resistance. Nonetheless, it still is significantly higher than what the analog designs offer.

The basic idea to achieve almost perfect efficiency is to never allow voltage potential and current flow happen at the same time between the transistors' drain and source terminals. Then, the product of drain to source voltage times drain to source current is always zero, which means no power is dissipated at the transistor, thus, all of it would be flowing towards the output. The power dissipation at the switch comes described by the following equation.

$$P_{diss} = \frac{1}{T_0} \int_{T_0} V_{SW} * I_{SW} dt \tag{4.1}$$

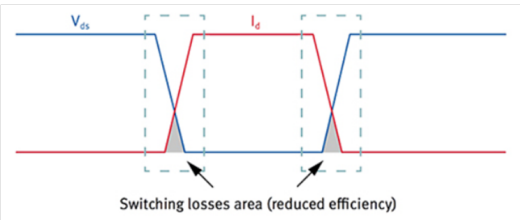

(a) Usual switch operation with non ideal edges

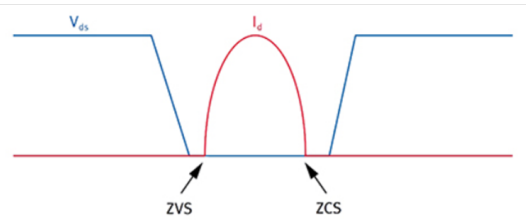

(b) Transitions when ZVS and ZCS conditions are met, also called soft-switching

Figure 4.4: Voltage and current waveforms for transitions with both basic operation and when zero power dissipation conditions are met [4].

Then, to really achieve zero power dissipation at the switch, the previous equation must be equal to zero at any time. This means that, at the switching transitions, we need to make sure the ZVS and ZCS conditions are met. In other words, soft-switching has to take place. This way, the switch closes when the voltage is already zero, and it opens when the current is already zero. This conditions can be easily understood with the help of Figure 4.4.

The driving signal needed for switching amplifiers, to be connected to the transistor's gate terminal, can be a digital signal; this signal is usually a train of pulses at the required frequency.

Additionally to the previously explained, some corrections can be made if the amplifiers are configured in differential mode. A differential topology is possible if two switching elements are used in a symmetric design with one of them being driven by the inverted driving signal. The output voltage would be taken between the outputs of each of the amplifier branches. Differential topologies, apart from being more complex, have several advantages in terms of avoiding interferences or noise since they would be cancelled for being present on both sides. This configuration, however, is left for future steps of the project and a single ended approach is addressed in this work. Figure 4.5 is an example of a differential, class E amplifier offered by the company EPC.

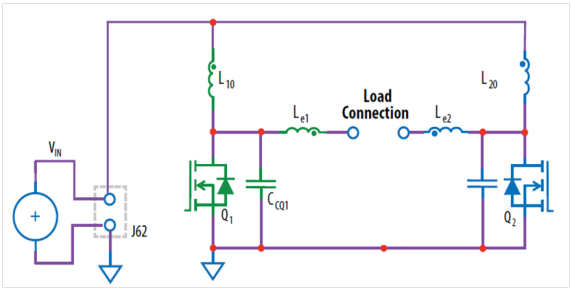

Figure 4.5: EPC9051 differential, class E power amplifier simplified schematic [5].

Class E power amplifier

The class E is the specific amplifier topology chosen to be implemented for our system. This amplifier has a potential theoretical efficiency of a 100% and its basic circuit structure, for its single ended configuration, can be seen in Figure 4.6a. The ideal current and voltage waveforms at the transistor, for one cycle, can also be observed. As explained before, the ZVS and ZCS conditions would be met in ideal conditions.

Taking a look at the elements that form the amplifier circuit, $Q1$ is a GaN FET doing the switching function while being driven through its gate terminal by a pulsed signal at the required frequency. The constant voltage source (V_{IN}) provides the power to the amplifier through a choke inductor ($L1$ in the schematic) that ensures a bias DC current level. Then, coil $L2$ and capacitor $C2$ form a resonator at the application frequency that acts as a short circuit at the fundamental frequency and as an open circuit at the rest of the harmonics. This avoids loosing power with all the harmonics that are not of interest.

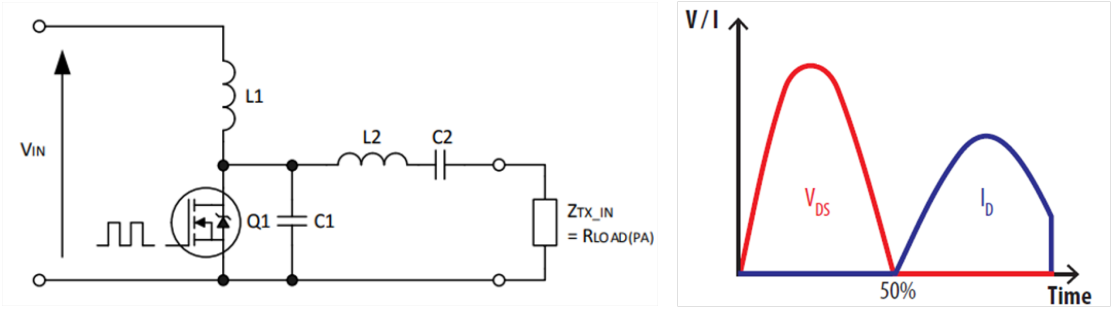

(a) Single-ended, class E amplifier basic schematic.

(b) Ideal waveforms at the switch (GaN FET)

Figure 4.6: Single-ended, class E amplifier and ideal operation [5][6].

Capacitor $C1$ is placed in parallel to the switch to allow the resonator pull AC current to make a full sine wave when the switch is open, as seen in Figure 4.7. Z_{TX-IN} is the load impedance.

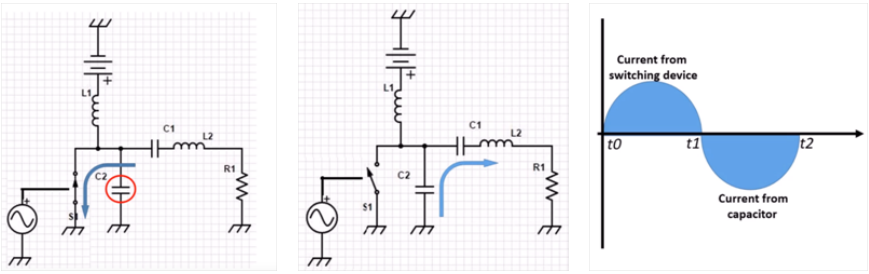

(a) Switch closed

(b) Switch open

(c) Output sinusoidal current

Figure 4.7: AC current flow in each of the switching scenarios

The application's frequency, load and power requirements are the ones that determine the values for each of the previously mentioned components. The basic approach assumes a duty cycle for the driving signal of 50%, and a real impedance as the load. The relationships that define the circuit elements under these conditions are depicted below [23].

$$V_{DD} = \sqrt{1.734 * R_{load} P_{out}} \tag{4.2}$$

$$C_s h = \frac{1}{5.447 * \omega R_{load}} \tag{4.3}$$

$$L_e = \frac{1.1525 * R_{load}}{\omega} \tag{4.4}$$

Then, C_s is calculated to resonate with L_e through the relation:

$$C_s = \frac{1}{L\omega^2} \tag{4.5}$$

As it can be observed, the load impedance is important for the calculation of the rest of

the components. The class E basic structure tends to deviate substantially from ZVS for small load variations, hence, the need of building an amplifier that allows proper operation among a certain range of load values.

Another issue to take into account is that these amplifiers produce high voltage and current levels that demand high limits of operation of the switching devices. Effort is being put to manufacture transistors that can handle high power at the same time as high frequency operation and good switching characteristics. This is the main reason why GaN FETs are starting to predominate in this sort of applications.

4.2 Variable load class E amplifier design and simulation

As found convenient in the previous section, providing the class E power amplifier with variable load operation is a must when dealing with applications where this load can change. It is very sensitive to load variations and performance would be dramatically degraded when its value is not the one for which it was designed.

Following the findings published in [24], the addition of some elements in the basic class E amplifier circuit presented in Section 4.1 can achieve this goal. The calculations to adapt the proposed modifications to our application are described in this section. Afterwards, a validation through schematic simulation is performed.

The selected approach provokes quite simple modifications to the basic schematic to achieve the aimed objective. It is assumed that the selected transistor offers good enough performance and 50% duty cycle. As it can be observed in Figure 4.8, the most important element added is a parallel-tuned output filter formed by L_P and C_P. Then, additional considerations are taken into account when calculating the components' values.

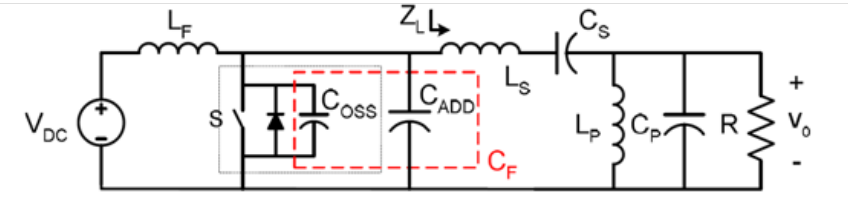

Figure 4.8: Modified schematic of the class E inverter with a parallel-tuned output filter

The switching device's output capacitance is going to be taken into account when selecting the value for C_{ADD}. The total capacitance value is named C_F, which is going to be of importance when calculating L_F's value.

The first step considers the output characteristics needed. Power, minimum and maximum load resistance, and input DC voltage are approximately related in the following way:

$$\frac{P_0 R}{V_{DC}^2} = 1.32 \tag{4.6}$$

Here, R_{min} will determine the output rated power and, R_{max} will determine the power

minimum value.

Then, an important design consideration is tuning both C_S, L_S and C_P, L_P networks to both resonate at the switching frequency f_0, 6.78 MHz. This is done to keep the load impedance mainly resistive.

$$\frac{1}{\sqrt{C_P L_P}} = \frac{1}{\sqrt{C_S L_S}} = 2\pi f_0 \tag{4.7}$$

Having two degrees of freedom here, it is recommended to choose the parallel network to provide filtering for the largest resistance, and the series network for the smallest load. The load is related to the filter by means of the quality factor, where $Q \approx 5$ would be selected for adequate filtering, then, the expressions would be:

$$\frac{R_{min}}{\sqrt{C_P L_P}} = \frac{\sqrt{C_S L_S}}{R_{max}} = Q \tag{4.8}$$

Finally, for the input network formed by C_F and L_F, the soft-switching condition has to be kept in mind. For that reason its resonating frequency is tuned to be just below 1.5 times f_0.

$$\frac{1}{L_F C_F} = 3\pi f_0 \tag{4.9}$$

The characteristic impedance of the C_F, L_F network was selected based on the minimum load resistance:

$$\sqrt{\frac{L_F}{C_F}} = k_f R_{min} \tag{4.10}$$

where k_f is a design constant with a value around 1. When selecting it, one starts with a low value of 0.5 and it is increased as much as possible while maintaining the ZVS condition.

Then, the elements calculation starts with the application requirements of power, load and frequency. In the treated case, the frequency to be used was 6.78 MHz, and the output power was selected to be 20 Watts, enough to charge a couple of phones. The load would be mainly resistive and oscillate between 8 Ω and 80 Ω, which would be the coil's parasitic resistance. Since our transmitter is an LC resonator, at the transmitting frequency, it acts as a short circuit and the resistive load is the only one left.

The Matlab code provided in Appendix B was used to calculate the values of all the components by using all the equations previously presented. The values obtained and needed for the schematic design are summarized in Table 4.1.

Then, the amplifier circuit was built in the ADS simulation environment for design validation.

First, in order to compare it against the variable load topology, a simulation with a basic amplifier structure without variable load support was performed. The main result to be observed is the voltage and current along one period at the transistor terminals. The obtained shape should be something similar to the presented in Figure 4.6b, where

Parameter	Value	Units
f_0	6.78	MHz
P_out	20	W
R_{min}	8	Ω
R_{max}	80	Ω
V_{DC}	11	V
L_F	136.93	nH
C_{ADD}	1.678	nF
L_S	0.94	μH
C_S	58.685	nF
L_P	0.376	μH
C_P	1.467	nF

Table 4.1: Variable load, class E amplifier values calculated for its components.

voltage or current are equal to zero when the other is not.

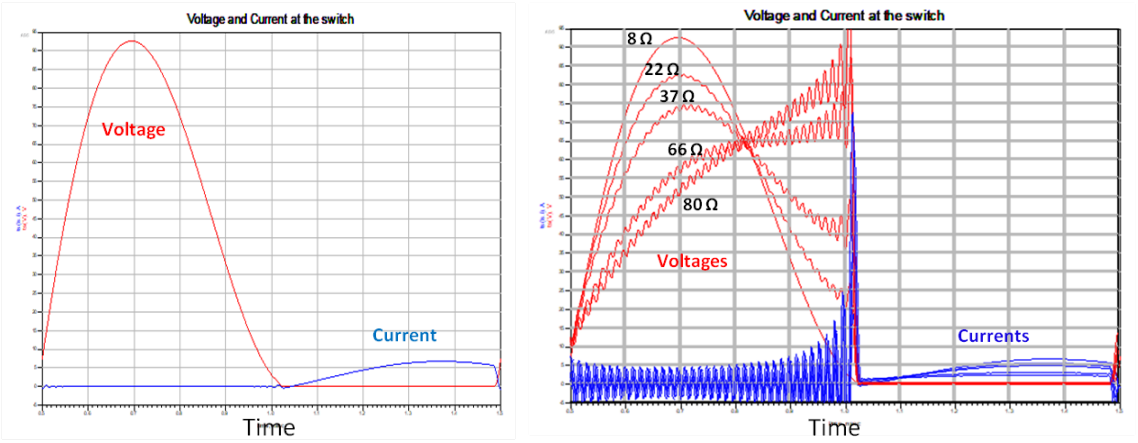

(a) Design case results.

(b) 8 to 80 Ω load resistance sweep results.

Figure 4.9: Class E amplifier ideal switch voltage and current simulation results.

Figure 4.9a shows the obtained result and what was expected. The waves have the right shape and current and voltage do not coincide in time.

Figure 4.9b shows what happens when a variable sweep is performed without modifying the amplifier. The results for different values of the load resistor between 8 Ω and 80 Ω show how the amplifier does not work in the desired regime when the load is not the design one. In this case, the switching becomes hard-switching, being the voltage forced to go down to zero by the switch, it is not zero at the switching instant anymore. Some ripple that gets bigger when the load gets further away from the design value can also be appreciated. The current has an undesired peak at the switching instant.

The variable load resistance amplifier shows different but appealing results when proceeding with the same simulation. This time, for the whole range of resistances, the behavior is always closer to the soft switching condition. The 8 Ω case is still the best one.

Regarding the voltage evolution, the one that was degrading more rapidly before, this approach shows how stable it is with the load change. It always returns to zero before

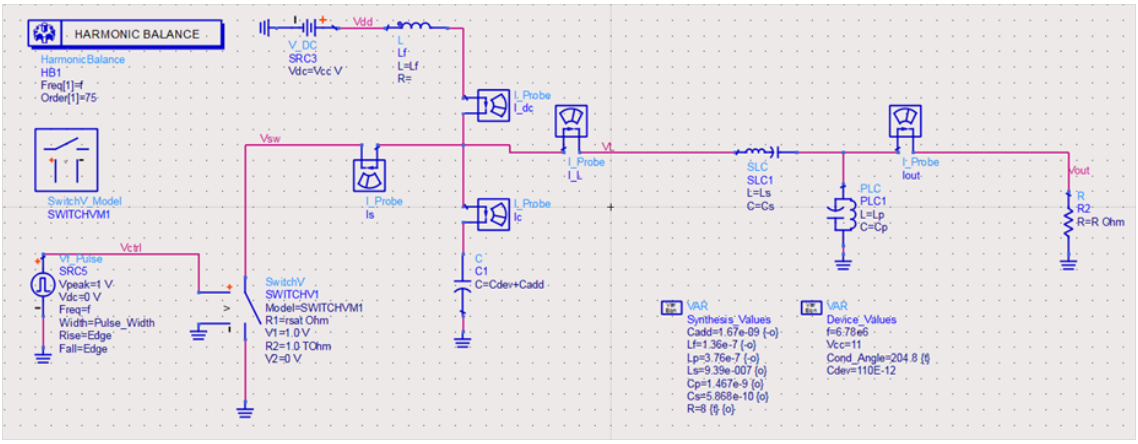

Figure 4.10: Variable load resistance amplifier schematic built in ADS software for simulation.

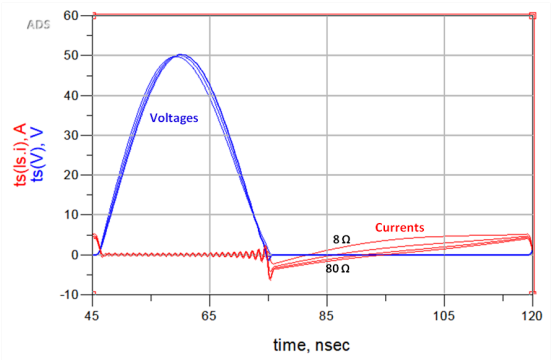

(a) Voltae and current waveforms at the switch for the different values of R_{load}.

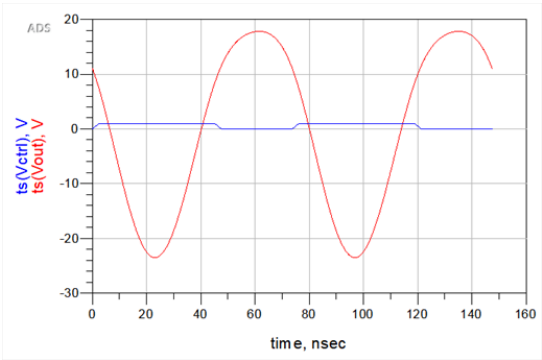

(b) Control signal and output waveform for the 8 Ω case.

Figure 4.11: Simulation results for the variable resistance, class E power amplifier.

closing the switch. The current is the price to pay here. At the instant the switch is closed, the current is negative and needs some time to become positive again. It is believed that the L_P, C_P resonator is the one allowing this current flow. The is also some small ripple when the switch is open, which will also affect the efficiency.

Observe, additionally, that the duty cycle has been modified for this simulation, where the switch is open for shorter time than it is closed. It was a manual adjustment made to allow the amplifier meet the ZVS condition.

Figure 4.11b shows the control signal, with this duty cycle modification appreciable, and the output voltage of the amplifier. The obtained wave would be adequate for a wireless charging scenario, but it has the drawback of not being perfectly symmetric due to the mentioned not symmetric control signal.

Finally, a power efficiency analysis was performed observing the dissipated power at the switch, calculated through equation 4.1.

Figure 4.1 shows when power is dissipated with the proposed scheme with all the resistor values simulated at the same time. Then, an integration of the dissipated and output powers was performed for each of the resistance values simulated. Finally, the efficiency evolution for the different loads could be plotted. All this is shown in Figure

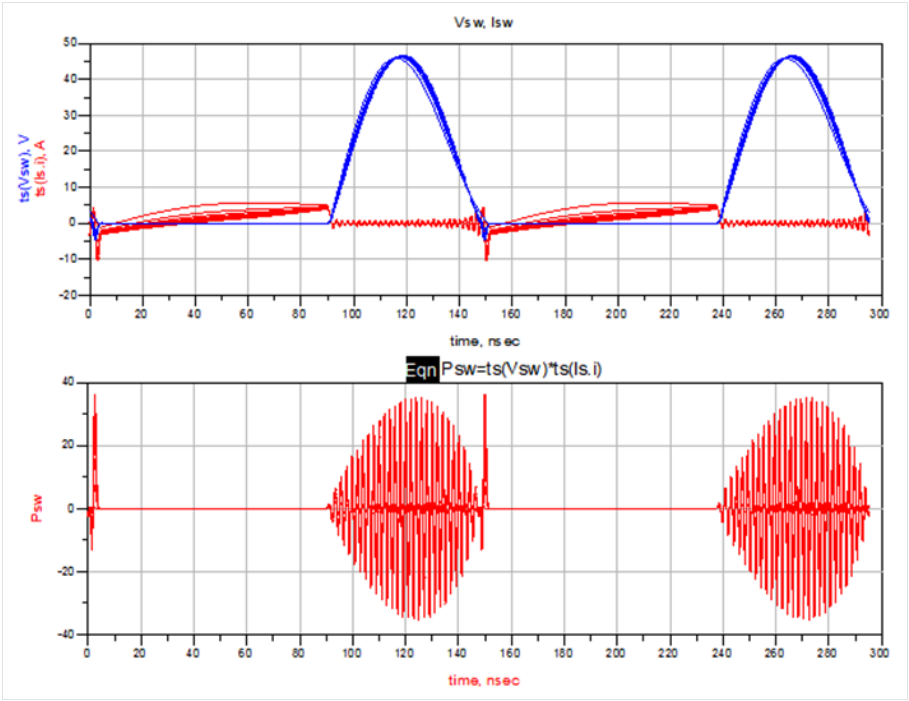

Figure 4.12: Voltage and current waves and dissipated power at the switch during two periods.

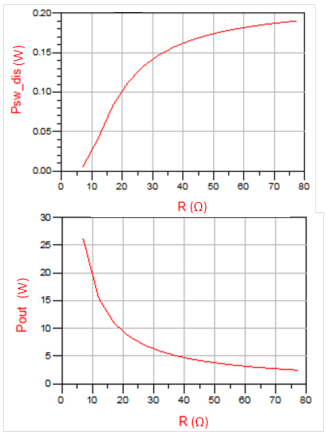

(a) Period integrated output and dissipated power at the switch versus the load resistance.

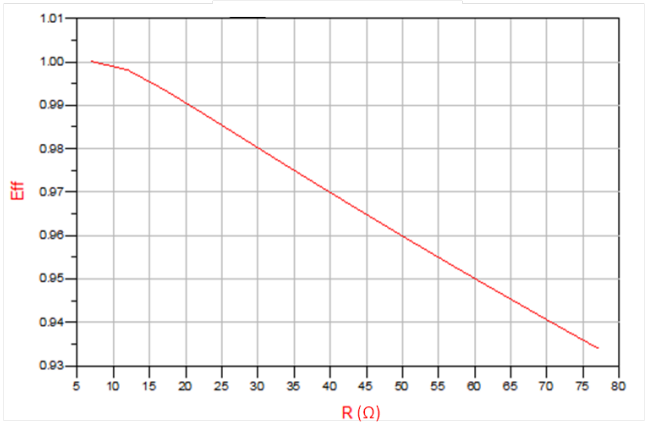

(b) Power amplifier efficiency along the load resistance range.

Figure 4.13: Power integrals and efficiency profile for the designed load range.

4.13.

The results obtained were favourable, with the performance decaying when the load gets further away from the original value, but still maintaining a very good efficiency level, being more than 90% for the whole operation range. An interesting observation is the practically linear evolution of the efficiency with the load change.

It has to be recalled that the switch used is ideal, which leads to this performance. The improvement compared to the basic amplifier structure, then, has been verified.

4.3 Summary and future steps

The need of an efficient and flexible amplifier continues being important during any test when elements or variations are added to the system. The variable load amplifier simulations show how a performance closer to the desired one can be achieved with the introduced circuital modifications. The waveforms at the switch can be clearly improved for a specific range of resistive loads as demonstrated. The trade-off here is the amplifier's increased complexity, further to ideal waveforms, lower efficiency than the standard class E amplifier topology, and even more sensitivity to frequency variations since more elements depend on it.

The immediate next step to continue with the amplifier's development would be its layout design on a PCB and fabrication for real testing. Afterwards, deciding the exact load range of operation, or impedance matching design depending on the use case of the amplifier shall be carried out.

Chapter 5

Magnetic Resonance Beamforming

As aforementioned before, beamforming is a technique used in RF communications to enhance a system capabilities provoking constructive interferences at the point where the receiver is localized. This, adapted to the WPT scenario, can be useful to enhance transmitted power and area coverage. In particular, it would be helpful for better coverage of the spaces left between transmitting coils in the charging surface intended application (red highlighted areas in Figure 4.1).

In this chapter, a brief explanation of how this technique works is presented, as well as some simulation results that verify its usefulness and a simple experiment.

5.1 Beamforming basics

The use of beamforming in MR WPT systems is proposed in several studies [7] [8]. The parallelism to RF BF helps to better understand its components and behavior.

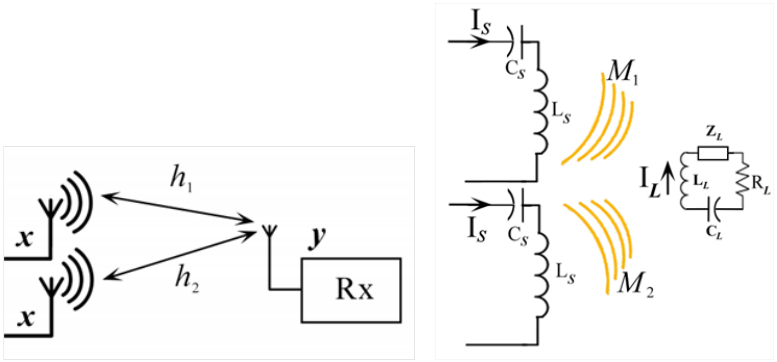

(a) RF BF system scheme. (b) MR BF system scheme.

Figure 5.1: Beamforming schemes parallelism [7].

In the conventional beamforming scenario, the received signal y is the summation of the transmitted signals (x) modeled by each channel (h_1 and h_2):

$$y = (h_1 + h_2)\, x \tag{5.1}$$

The same transmitted signal - channel - received signal scheme can be followed in the magnetic resonance scenario. The current I_s plays the transmitted signal role, the channel modeling is going to be done through the mutual inductance between coils, and the received signal will be the current I_L.

$$I_L = \frac{j\omega}{Z_L + R_L} (M_1 + M_2) I_s \tag{5.2}$$

where, if $m_i = \frac{j\omega}{Z_L+R_L} M_i$, a similar expression is obtained:

$$I_L = (m_1 + m_2) I_s \tag{5.3}$$

Then, with the expression found, a beamforming vector (β_1, β_2) can be created to transmit $\beta_1 I_s$ and $\beta_2 I_s$, being:

$$\beta_i = \frac{m_i^*}{\sum_{i=1}^{n} |m_i^2|} \tag{5.4}$$

This way, adjusting the currents at the transmitters through the weights calculation, the beamforming action is achieved. In practice, these current adjustments would be translated through Ohm's law to voltages for easier application, it is always easier to control voltages in a circuit instead of currents.

Regarding the phase of these currents, their effect is not the same as in RF BF. The reason is that the current itself is not what causes the power transfer, but the magnetic flux created at the transmitter and flowing through the receiving coil.

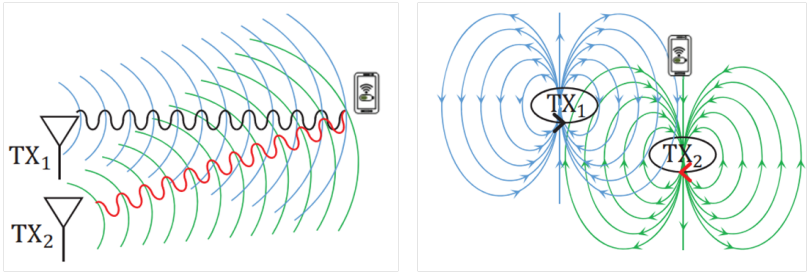

(a) RF BF phase diagram. (b) MR BF flux diagram.

Figure 5.2: Signal phase and magnetic flux difference in a beamforming scenario [7].

Magnetic flux's flowing direction is the important parameter, as if its phase could only be either 0^o or 180^o. When the AC current is in its positive part of the cycle in the transmitting coil, the flux travels in one direction according to the *righ-hand rule*. When the current flows in the opposite direction, so does the flux. Additionally, in the MR case, the channel impact is not the same as for the RF approach, where amplitude and phase are affected. Here, the channel just translates into relative position of the coils, not attenuated signals or shifted phases.

In the WPT BF scenario, the signals' phases at the transmitters, hence, are going to be either 0^o or 180^o depending on where the receiver is placed. The flux lines out of a coil (or magnet) follow a pattern like the one seen in Figure 5.2b. Depending on the receiver's

location, the caused magnetic flux is going to travel through it in one direction or the other. It is desired that the flux lines coming from several transmitters flow in the same direction at the receiver's location. This would create the aimed effect of "constructive interference".

It is important to highlight that this process requires a channel estimation phase previous to the weights calculation. Additionally, for this channel estimation, the transmitting coils' inductance values are needed, thus, a pre-calibration phase will also be necessary. With the inductance information, each coil's impedance can be calculated after measuring the current flowing through them when a known voltage is applied between their terminals. With all that, the mutual inductance, and then, the channel estimators m_i can be calculated. The following relationships are used for this calculation:

$$z_i' = \frac{V_{si}}{I_{si}} = z_{si} - j\omega M_i \frac{I_L}{I_{si}} \tag{5.5}$$

$$\omega^2 M_i^2 = \left(z_i' - z_{si}\right)\left(R_L + z_L\right) \tag{5.6}$$

Note that a current measurement step is required in the middle of the channel estimation process. This is another purpose for the sensing system proposed and designed in Chapter 3 of this thesis.

The block diagram that describes the actions that the beamforming process includes is depicted in Figure 5.3. See the *pre-calibration* and *channel estimation* phases just explained. After the voltages are applied, the process starts again from the channel estimation. The pre-calibration phase is a one time action.

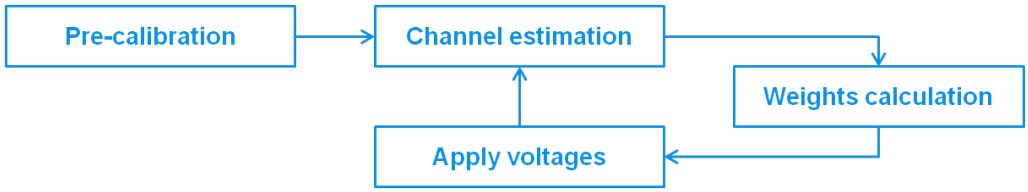

Figure 5.3: Block diagram of the bamforming process.

Because of this beamforming approach, where each of the transmitters has its own voltage (or current), all of them need their own power amplifier. Then, a simple but reliable power amplifier must be used in order to allow system scalability, miniaturization and reduced cost.

Then, this same approach can be addapted for the scenario where multiple transmitters charge multiple receivers at the same time. This is the case developed in [8]. The calculations are a bit more complex this time since the mutual inductances between all the devices affect the system performance.

The same equivalent circuits for transmitter and receiver are used in Figure 5.4, and the simple addition of multiple receivers adds complexity to the system variables and their calculation. Mutual inductances and impedances are treated with matrices and the

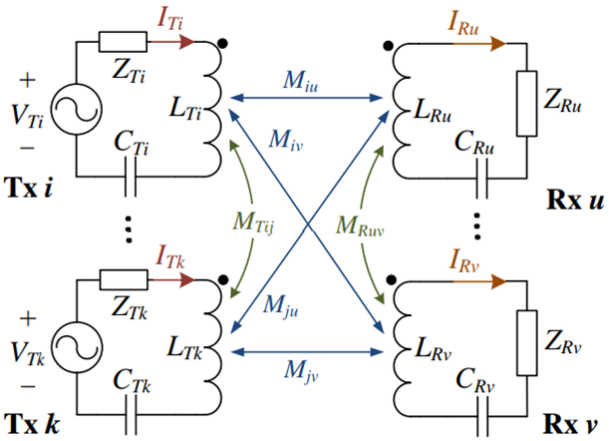

Figure 5.4: Multiple transmitter and multiple receiver scenario schematic and mutual inductances [8].

calculations are tougher. In the followed publication, the authors propose an adaptive algorithm to make the system predict the next values to avoid recalculation. The channel estimation step could be performed from time to time, just in case the scenario changes rapidly. The block diagram with the adaptive algorithm extra feature is depicted in Figure 5.5.

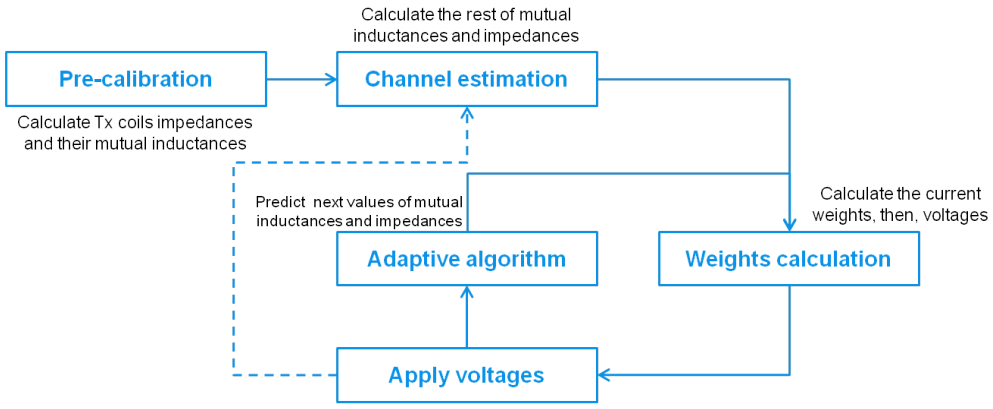

Figure 5.5: Beamforming process block diagram with adaptive algorithm to allow faster recalculation of the weights.

5.2 COMSOL simulations

The next step planned after understanding the MR BF technique was to simulate this environment. Using COMSOL Multiphysics, a simple scenario was created and a beamforming simulation was performed. This would help verifying the theory and making sure we knew how to follow the correct procedure. The simulations would also allow easy experimentation with different numbers of transmitting coils, as well as changing the transmitter and receiver coils physical characteristics.

The scenario would consist of five transmitting coils and a receiver. The main interest

was put in the magnetic flux distribution over the covered surface. At the receiver, the induced current and received power would be also monitored.

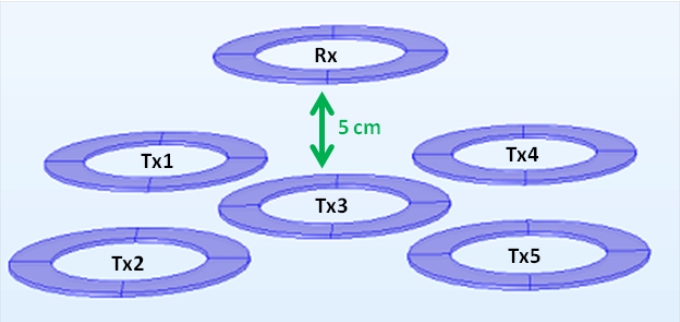

Figure 5.6: Beamforming scenario COMSOL Multiphysics setup.

Figures 5.7a and 5.7b the magnetic flux through a plane right above the transmitting coils. The shown results are extrusions of the 2D plots to emulate the beamforming effect. The plot height and colour are both proportional to the magnetic flux magnitude.

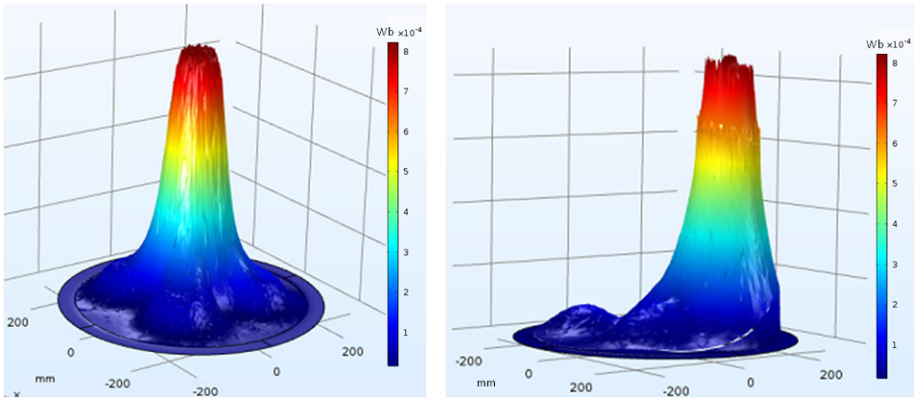

(a) Beamforming towards the surface's center.

(b) Beamforming towards a side of the surface.

Figure 5.7: Magnetic flux intensity results obtained with COMSOL.

Observe how the magnetic flux is concentrated in certain areas and not all over the surface. That is a convenient behavior in order not to waste energy and loose efficiency, and for security purposes, being sure the energy can be sent to certain devices and not affect others (RFID tags could be damaged for example).

Some other variations on the setup allowed understanding a little better the effect of some variables on the system performance. For example, regarding the transmitters' dimensions, using more and smaller transmitters allowed better directivity and efficiency, but less maximum power transferred and the system becomes more complex because of the additional hardware. This setup is shown in Figure 5.8a.

Measurements at the receiver's resonator terminals allowed calculating the power transfer efficiency. Although the values obtained were lower than expected, they gave valuable information about better and worse situations. Regarding the receiver size, the results showed higher efficiency the bigger the receiving coil was, which made sense, while being

smaller than the transmitters' coils. See Figure 5.8b.

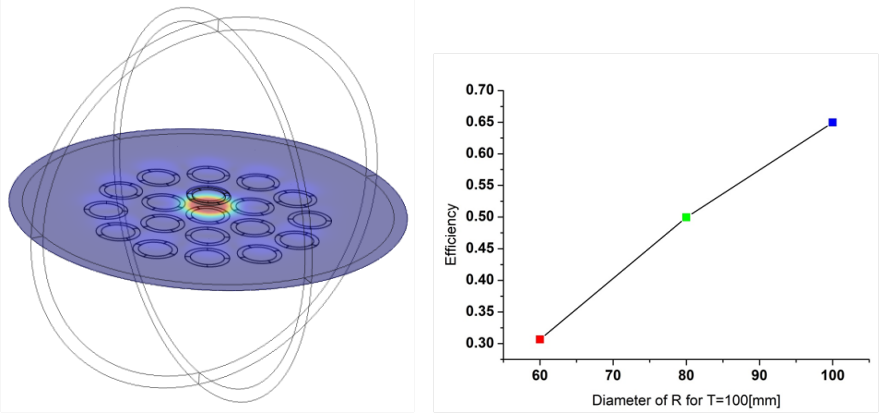

(a) More and smaller transmitters simulated scenario.

(b) Efficiency versus receiver size.

Figure 5.8: Additional cases simulated with COMSOL.

More specific tests might be performed in the future once the application's dimensions, power, and distance requirements are more clear. These COMSOL simulations showed how useful this software can be for the development of a system like this charging surface with beamforming capability.

The software might offer the possibility of implementing many other features such as automatic control of the beamforming, receiver movement, simulations at several distances, alternative transmitters distribution, simulations over time, RFID interferences, etc. The simulation environment is ready for the future implementation of any of the mentioned additions whenever it is needed as the project advances.

5.3 Beamforming Proof of Concept

A very basic experiment was performed to first validate the beamforming effect. The aim here was not to implement IT with all its steps and elements to get the best transmission possible, but to simply observe that some improvement was achieved when trying to charge a receiver in an area where it would be difficult without this technique. The pre-calibration and channel estimation stages were not done. The values of all the elements in the system were known.

The test would be performed with low power signals, just observing that the received voltage would experiment changes when comparing the non-beamforming and the beamforming setups.

The transmitters and receiver used were copper coils from a wireless charging kit for evaluation. The transmitted signals came from an Analog Discovery 2 device which allowed to synchronize both of them and set the desired phase difference between the two applied signals. The frequency used was 2 MHz due to the Analog Discovery's limitations and the measurements would be taken with an oscilloscope.

In the experiment, the main interest was to measure the signal at the receiver when

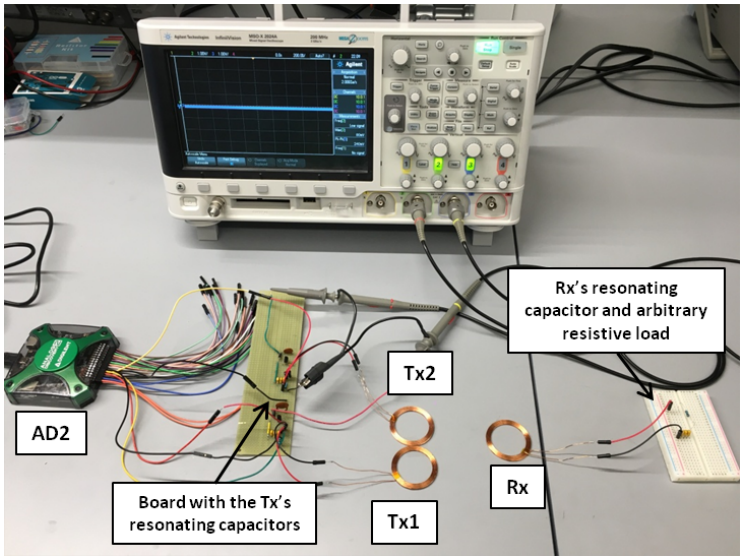

Figure 5.9: BF proof of concept experiment setup.

it was placed in the middle position between the two transmitters. The phase difference between the two transmitted signals would be changed 180^{o} to detect the worst case and the best case.

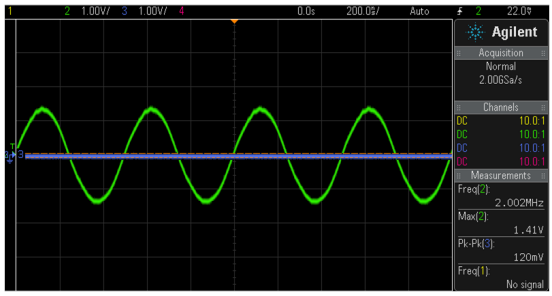

(a) Voltage at the receiver with phases 0^{o} and 180^{o} at the transmitters.

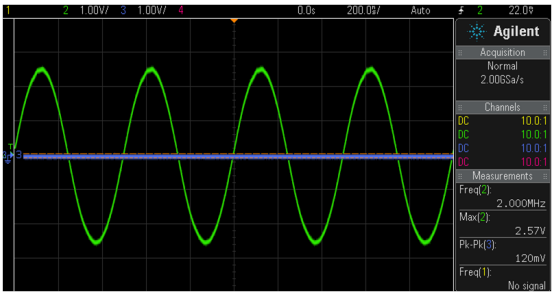

(b) Received voltage signal with 0^{o} phase difference between transmitted signals.

Figure 5.10: Oscilloscope measurements of the gathered signal at the receiver.

In the results, the worst case of 1.4 V corresponds to different phases: 0^{o} for Tx1 and 180^{o} for Tx2. The best case, with 2.8 V, corresponds to equal phases. This result made sense since, with the receiver at the same distance from both transmitters, the magnetic flux flow follows a symmetric pattern. When the receiver was placed right over one of the transmitters, different phases would give the best results.

It has been demonstrated how, just operating with the phases, the received signal intensity would change. That, applied with all the previously described steps and in a more complex application with more coils involved, would become the aimed BF-MR WPT system. The beamforming proof of concept did succeed.

5.4 Summary and future steps

Beamforming was found to be a good addition to our aimed MR surface charging system. Its performance enhancement made it really appealing and the first steps towards starting its implementation were set. Understanding the phenomena and how to control it, performing the first simulations and, eventually, demonstrating its effect with a simplified experiment were the tasks undertaken. A good basis was set in order to continue progressing with this topic.

On the other side, the simulations and experiment also showed the complexity of this approach. Many parameters need to be measured or calculated with precision, the multiple receiver scenario is still to be better analyzed, and a real experiment with powerful signals might introduce even more challenges. More exhaustive and complex COMSOL simulations would also be needed to continue with the progress. Appropriate amplifiers, sensing circuits, voltage and current regulators and fast calculations, for example, would be required for a real implementation. A good beamforming performance needs of many other elements working precisely at the same time, a complex and laborious task.

Chapter 6

Energy Hopping Using a Planar Array of Coils

Towards the end of the project, the energy hopping concept was found in the literature. It would bring the possibility of covering large areas for charging, and with a very simple structure composed of short-circuited resonators distributed in a planar array format.

It was decided to get deeper into this topic and build a prototype that reproduced that phenomena and allowed better understanding of the opportunities it could bring and its limitations. The aim was to perform the preliminary steps for future development of this approach if found useful.

6.1 Energy Hopping Concept

In order to improve the channeling of the magnetic field in resonance condition, arrays of intermediate resonators have been introduced between the transmitter and receiver coils [25] [26]. Different arrangements have been proposed; for example, arrays may be made with the resonators along a line or in a plane and with the receiver coil sliding over them.

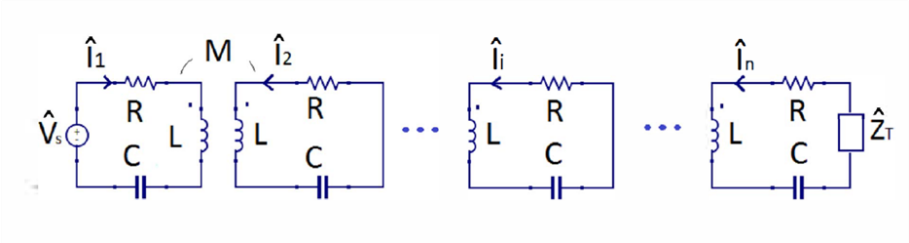

Figure 6.1: Planar array circuit schematic representation.

The Magneto-Inductive (MI) wave theory that explains the phenomena has been studied by several authors [27] and is what allows the energy hopping effect from coil to coil. The resonators are composed of a short-circuited loop with coil and a capacitor resonating at the transmission frequency. Each of them is modelled by an inductance L and a capacitance C, the loop's intrinsic resistance R, and coupled to its nearest neighbours

by a mutual inductance M. Note that the couplings between nonadjacent resonators are neglected. The first loop is supplied by a voltage source V_s, and the last one is loaded with an impedance Z_TObserve Figure 6.1.

For the ideal lossless case, an MI waveguide approach allows calculating the transmission's parameters in a simple way. First, Kirchoff's voltage law yields a relation between the currents in each loop:

$$ZI_n + Z_m\left(I_{n-1} + I_{n+1}\right) = 0 \tag{6.1}$$

Where $Z = j(\omega L - 1/\omega C)$ is the loop impedance and $Z_m = j\omega M$. Assuming a travelling wave solution as $I_n = Iexp(-jkna)$ then, with propagation constant k and loop separation a, from equation 6.1 we obtain:

$$Z + 2Z_m cos(ka) = 0 \tag{6.2}$$

Then, if we assume the frequency is ω_0, in the middle of the band, $ka \approx \pi/2$. Finally, the ideal power P carried by the wave at the resonant frequency is:

$$P = \left(\frac{\omega_0 M I^2}{2}\right) \tag{6.3}$$

Additionally, the MI theory in [28] showed that at the resonance frequency, and for an infinite low-loss line, the efficiency can be maximized by having $Z_T = \omega_0 M$.

All these relationships show how helpful the transmission line analysis thechniques can be for this sort of application. Observe, as well, how important mutual inductances are here, as expected.

The two main cases studied for energy hopping differ in the resonators orientation relative to the power flow direction. On the one hand, arrays formed by concentric resonators that transfer the energy perpendicularly to the coils' planes as in Figure 6.2a [29]. On the other hand, resonators can be placed as a row or matrix on one plane and transfer the efficiency along this plane , as Figure 6.2b depicts [30].

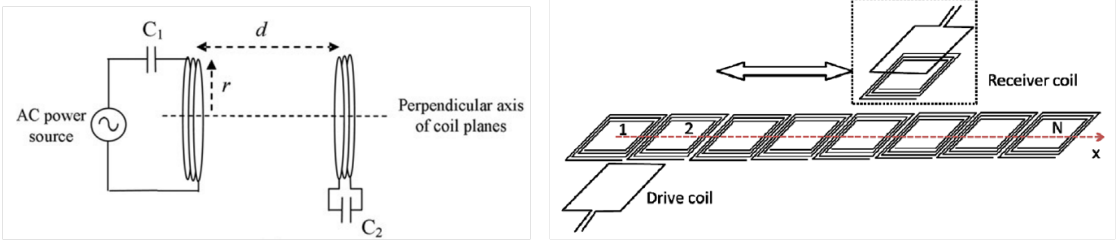

(a) Perpendicular transmission setup. (b) Planar array configuration.

Figure 6.2: Two different ways to configure the resonators' distribution for the energy hopping phenomena.

Additionally, studies such as [28], [29] show how this energy hopping effect can be split in different paths or forced to follow curves, for example. It has been mainly studied in

the case of perpendicular transmission of the energy, and could possibly be of interest in specific WPT scenarios.

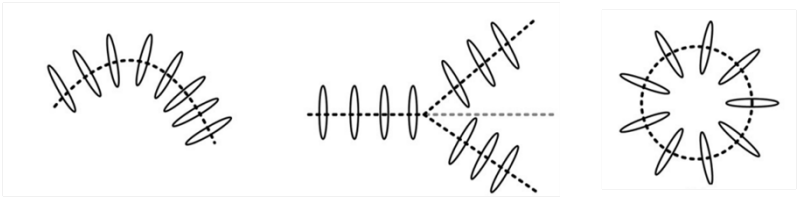

Figure 6.3: Examples for different power guiding configurations.

6.2 COMSOL Simulation

In the same way as performed for the beamforming technique explained in Chapter 5, after understanding how the energy hopping phenomena works, a COMSOL Multiphysics simulation was built in order to better visualize its effect. Then, the simulation environment would be ready for the addition of other features, experimenting with specific characteristics of the system, or whatever the project requires for continue with its development.

The simulated scenario can be seen in Figure 6.4, where all the resonators are placed on the same plane and one next to the other. The transmitter here is right under the first resonator, and the receiver above the last one.

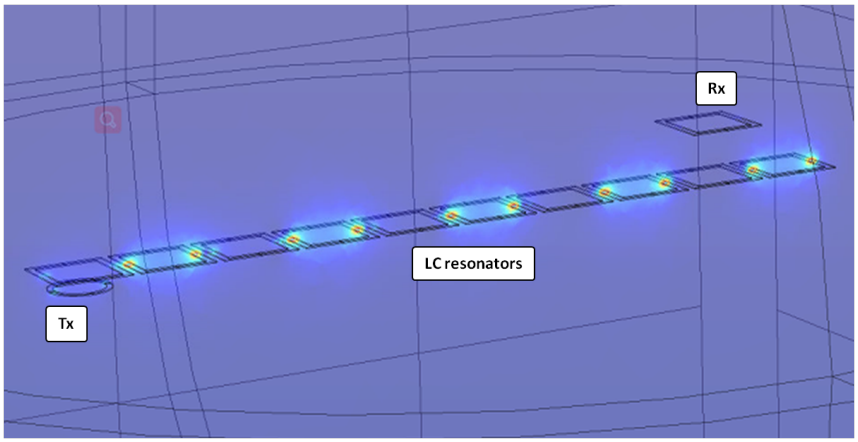

Figure 6.4: COMSOL 3D design of the planar array of coils for energy hopping.

These simulations wanted to simply show how the phenomena is a reality and that the energy can be transferred through the resonators to the receiver. In a second simulation, the first of the resonators was replaced by the transmitter. As expected, the power transmission also worked.

In Figure 6.5b, a magnetic field pattern can be appreciated as the energy flows along the resonators towards the receiver. Remember this magnetic field's sign directly depends on the current flow direction in each of the coils.

The receiver would get energy although the efficiency results did not show the expected values. This might be due to the short-circuit configuration of the resonators, where the

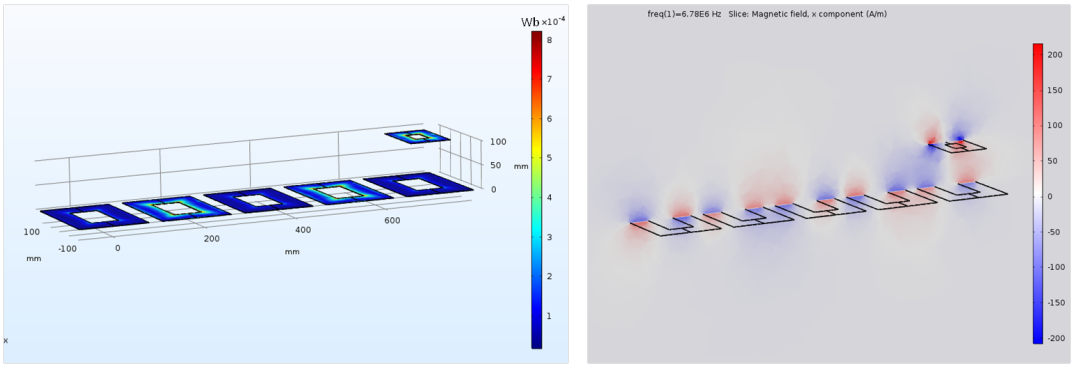

(a) Magnetic flux on the coils' surfaces simulation results.

(b) Magnetic field X component on the vertical section to appreciate the flow pattern.

Figure 6.5: Planar array with transmitter on the resonator's plane COMSOL simulations.

software would find some incompatibilities depending on how they were implemented. The efficiency was known to be higher as the energy hopping phenomena had already been described in some other works. In future revisions of the simulation environment, the coils and capacitors configuration should be improved in order to get closer-to-reality results. However, a functional simulation was built that would be able to tell what changes in the system could be critical or would not even affect the charging action.

6.3 Experimentation

Several identical nuCurrent MR transmitting coils with their resonating capacitors were purchased in order to allow reproducing the coil array energy hopping experiment. One of the resonators was left open to be connected to a power amplifier, and the rest of them were short circuited, just being a coil and its resonating capacitor in series, to act as repeaters.

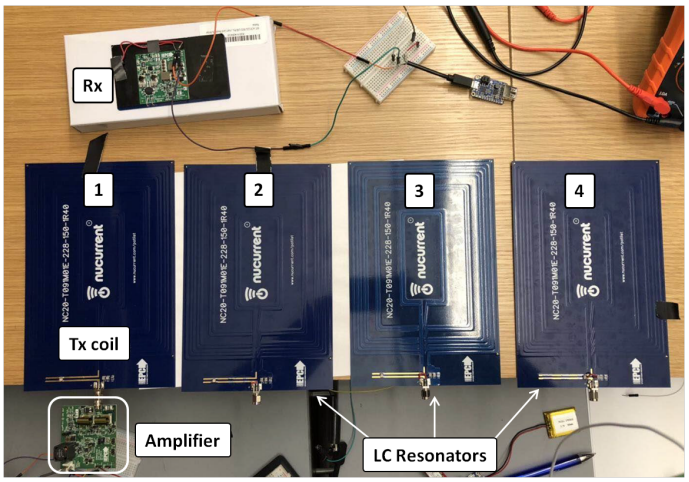

Figure 6.6: Planar array row setup with four coils.

The amplifier and the receiver would be the same ones used in the sensing experiments

in Chapter 3. Due to the amplifier and test characteristics, the coupling between coils would make load seen by the amplifier be out of the ideal operating range, thus, the end-to-end efficiencies were expected to be lower than the 20% obtained with normal operation. The positions where the receiver would charge and the transmission efficiency would be the two main features analyzed.

One experiment had an identical setup to the simulation case shown in Figure 6.5, with the transmitter in the first position of the planar array. The charging characteristics would be observed when placing the receiver along the row of resonators. The first parameter observed is the drawn current by the amplifier.

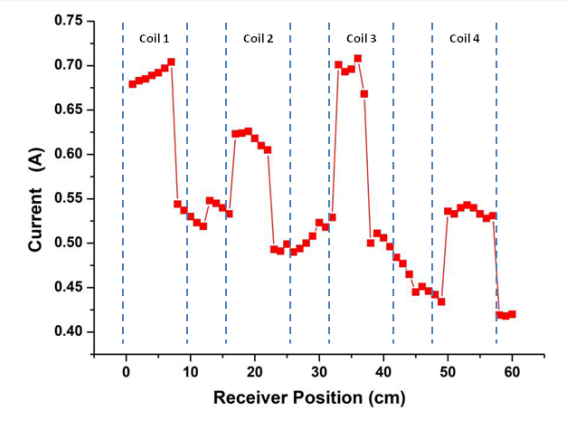

Figure 6.7: Current drawn by the transmitter's power amplifier along the planar array composed of four coils.

From this results, it can be clearly identified the instants at which the receiver is charging the battery due to the abrupt changes in the current consumption. From this, then, some facts can be extracted. The first and most evident observation is that we achieved charging the receiver's battery over any of the coils in the array. As a negative but expected point, it would never charge in between coils.

Secondly, the current does not have a value for charging and another for not charging, they are always different, what brings us to the conclusion that the position of the receiver along the array affects the load impedance all the time. Since the amplifier is never working under the same conditions, the currents change. As a general trend, it becomes lower when the receiver travels away from the transmitting coil, reducing its influence on the system.

A final observation is that, from measuring current only at the first coil, the receiver position cannot be determined. A receiver charging on the fourth coil had the same impact as a receiver not charging between the first and second coils.

Then, the received power was measured and used to calculate the end-to-end transmission efficiency when the receiver was charging with its coil concentric to each of the coils in the planar array.

From the plots in Figure 6.8, we can first see how higher received power does not mean better efficiency. The first coil gives the most power to the receiver, while the coil that allows the system perform more efficiently is the fourth one (except for the 4.5 cm

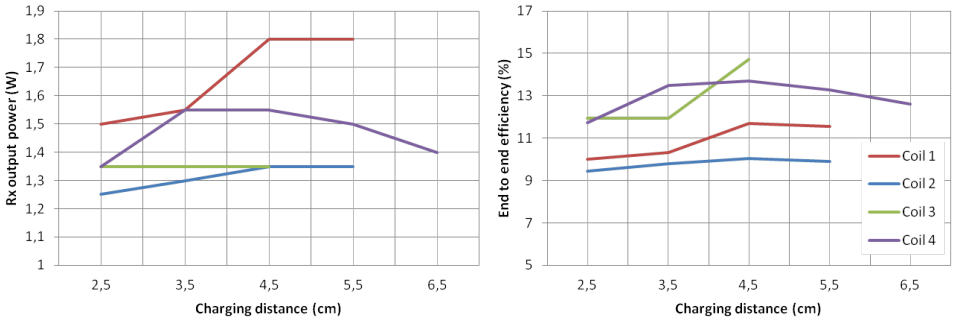

Figure 6.8: Power and efficiency against charging distance measurements for each of the coils in the planar array.

measurement at the third coil, which is believed to be a measurement error). Regarding the low efficiency values obtained, it has to be said that, the highest efficiency achieved with the available hardware, has been 20% as shown in Sections 3.2.2 and 3.3.2.6. Compared to that value, 50% of the efficiency is lost when implementing the energy hopping approach, which is a considerable loss, but allows the system to charge a receiver and is a promising result towards future development, being this a first proof of concept implementation.

Interestingly, the second coil is the one that offers the worst behavior regarding both received power and efficiency. Oppositely to what intuition would have said, the performance does not necessarily degrade with the number of "hops" the energy has to go through.

Regarding the vertical distance of charging, the fourth coil offered the best response here as well, allowing to charge with the receiver 6.5 cm far away from the surface. The worst coil regarding this feature was the third one, only charging up to 4.5 cm.

It has to be said that, when changing the number of resonators in the row configuration, the overall best case would always happen when charging over the last coil.

Finally, some other tests observing the same parameters were performed but changing the configuration of the planar array. The matrix configuration was tested to verify its performance.

The X and Y axes represent the charging surface plane. The efficiency values were very similar to the previous configuration, around 10%. The power could travel in both X and Y directions. The most interesting phenomena observed was the no charging over coil 2. There certainly was some power but not enough to allow the battery charger work properly. Here, again, the coil with the best performance was the one situated the furthest away from the amplifier-connected coil.

6.4 Outcome and forthcoming challenges

The energy hopping approach through the use of a planar array of LC resonators has been found as an option for future development of the MR charging surface. The first steps to understand the phenomena and the basis to continue improving this approach have been

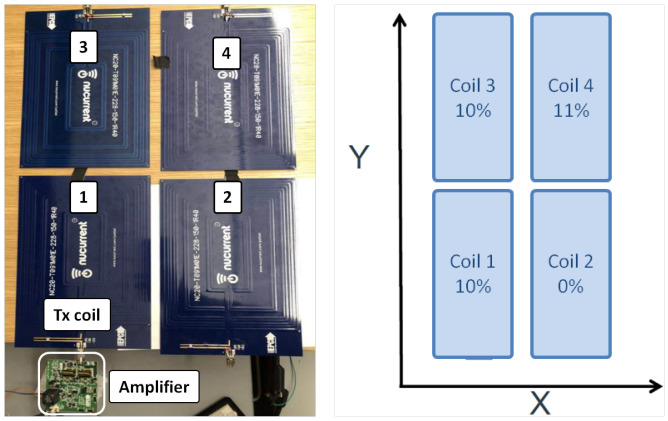

(a) Matrix experiment setup. (b) Matrix of coils scheme and efficiency measured.

Figure 6.9: Matrix configured planar array setup and efficiency results for each of the four coils.

settled.

It has been verified how the energy can be transferred with a long range of operation with a reasonably simple setup. Resonators are easy to build and passive, so the hardware and cost scalability this approach offers is its main advantage. Another great feature is that the efficiency does not decay when the number of hops from coil to coil increases, which potentially allows covering very big areas.

On the contrary, many issues result from the use of this technology and when aiming a well rounded and robust system. The efficiency, even though it allows the receiver to be charged, is low, and the load effect on the amplifier is notorious. Mutual inductance is an important parameter to be taken into account and, in the same way as in the beamforming solution study, it was found to be difficult to measure. Difficulties show up with these systems when well characterized real experiments are required. Mutual inductances between coils and circuit parameters in the resonators are not easy to be measured, and good resonance precision is also not easy to achieve due to real components' tolerances.

Even bigger challenges come up when talking about sensing and regulation. There is no chance of using the beamforming approach to charge receivers placed in the spaces between coils since the resonators are passive and cannot be controlled. A big challenge would be finding ways to route the energy to different receivers and how to change the amplifier's behavior for the best possible charging performance. There is also no precise sensing capability to detect the receiver's position over the surface.

Summarizing, the energy hopping phenomena is a reality and it can be achieved with relatively simple hardware. However, the control and monitoring of an energy hopping system become big challenges and many improvements should be tested in the future. The inclusion of the passive sensing circuits presented in Chapter 3 with each resonator, making the resonators controllable through switches that turn them on and off, finding ways to emulate the beamforming effect presented in Chapter 4, or combining several amplifiers could be some research possibilities for the near future.

Chapter 7

General Conclusions

The thesis development has been experiencing continuous work plan modifications but the project scope has always been in the focus: to set the first steps in the understanding and development of elements needed to build a MR WPT system capable of charging multiple wearable devices placed over a large surface.

A sensing board has been developed and fabricated for taking voltage and current measurements over a square, 33 W, 6.78 MHz signal. Read from an MCU, the transmission voltage provides information about system failure, and the current measurement allows detecting the presence of a receiver over the transmitter's coil, experiencing a stable, detectable change of 0.2 V at the output. Then, a class E power amplifier for driving transmitting coils has been successfully designed and simulated for variable load operation. A load difference of 1 order of magnitude would still allow the amplifier work under the ZVS condition as desired. Finally, the beamforming and energy hopping variations for the aimed charging surface have been analyzed, simulated using COMSOL Multiphysics, and demonstrated through experiments. The simulation environments will provide the group with a handful tool for future development of these ideas. The beamforming experiment showed a 50% improvement on the received signal amplitude in the area between transmitting coils. The energy hopping phenomena has been demonstrated for a transmission with four hops through a planar array of resonators.

Nonetheless, it has been seen how, in each of the topics treated, adding complexity and system robustness easily becomes a big challenge. Thorough characterization, and intensive simulation and testing would be required, as well as exploring other additional features. Further development is still needed before combining the elements studied within one system.

Regarding the general skills-related lessons learned, the project has appeared to be very fruitful. Due to the fact that a completely new topic had to be introduced to the group, the whole process of browsing in the literature, understanding the theory and basic principles, deciding which approaches would be more appropriate for the aimed application, and predicting how far we could get with the development of each of the ideas were all big challenges. Simplification and focus on specific topics helped with the progress, instead of

trying to solve everything at once. In addition, the fact that the final aim was a potentially commercial product also dictated some characteristics, such as having to be realistic and guaranteeing the feasibility of any proposed solution.

Bibliography

[1] W. J. Johnson Co. *Nikola Tesla, "Experiments with alternate currents of very high frequency and their application to methods of artificial illumination" in Electrical World magazine*, 1891. URL `https://commons.wikimedia.org/w/index.php?curid=5931982`. [Transferred from en.wikipedia to Commons, Public Domain; accessed Dec-2018].

[2] Wikipedia. *"Power Amplifier classes"*, last edited 2019. URL `https://en.wikipedia.org/wiki/Power_amplifier_classes`.

[3] Maria Guerra. *"Can Class-D Amplifier Audio Performance Get Any Better?"*, ElectricDesign, 2016. URL `https://www.electronicdesign.com/analog/can-class-d-amplifier-audio-performance-get-any-better`.

[4] Steven Keeping. *"A Review of Zero-Voltage Switching and its Importance to Voltage Regulation"*, Digikey article library, 2014. URL `https://www.digikey.com/en/articles/techzone/2014/aug/a-review-of-zero-voltage-switching-and-its-importance-to-voltage-regulation`.

[5] Efficient Power Conversion corporation. *"Demonstration System EPC9051 Quick Start Guide"*, 2016. URL `https://epc-co.com/epc/Portals/0/epc/documents/guides/EPC9051_qsg.pdf`.

[6] Peter B. Green. *"Class-E power amplifier design for wireless power transfer"*, Infineon Application Note, 2018. URL `https://www.infineon.com/dgdl/Infineon-Wireless_power_transfer_class_E_power_amp-AN-v01_02-EN.pdf?fileId=5546d46262b31d2e016351b8108a1c15`.

[7] Jouya Jadidian and Dina Katabi. *"Magnetic MIMO: How To Charge Your Phone in Your Pocket"*, MobiCom'14, 2014.

[8] Lixin Shi, Zachary Kabelac, Dina Katabi, and David Perreault. *"Wireless Power Hotspot that Charges All of Your Devices"*, MobiCom'15, 2015.

[9] Chen Li, Jeremy Warner, Ufuk Muncuk, Kaushik R. Chowdhury, and Stefano Basagni. *"REACH-Mote: A Range Extending Passive Wake-up Wireless Sensor Node"*, ACM Transactions on Sensor Networks, Vol. 11, No. 4, 2015.

[10] Ufuk Muncuk, Kubra Alemdar, D. Sarode, and Kaushik R. Chowdhury. *"Multi-band Ambient RF Energy Harvesting Circuit Design for Enabling Battery-less Sensors and IoTs"*, IEEE Internet of Things Journal, pp. 2700-2714, Vol. 5 , No. 4, 2018.

[11] Lu Xiao, Dusit Niyato, In Kim Dong, and Han Zhu. *"Wireless Charging Technologies: Fundamentals, Standards, and Network Applications"*, IEEE Communications Surveys and Tutorials, pp. 1413-1452, Vol. 18, No. 2, 2016.

[12] Wireless Power Consortium. *"The Qi Wireless Power Transfer System Power Class 0 Specification"*, Version 1.2.3, 2017. URL `https://www.wirelesspowerconsortium.com/`.

[13] AirFuel Alliance. *"AirFuel standard specification"*, 2016. URL `https://www.airfuel.org/`.

[14] Michael A. de Rooij. *Wireless Power Handbook.* Power Conversion Publications, 2015.

[15] Efficient Power Conversion corporation. *"Demonstration System EPC9129 Quick Start Guide"*, 2018. URL `http://epc-co.com/epc/Portals/0/epc/documents/guides/EPC9129_qsg.pdf`.

[16] Efficient Power Conversion corporation. *"Demonstration System EPC9515 Quick Start Guide"*, 2017. URL `http://epc-co.com/epc/Portals/0/epc/documents/guides/EPC9515_qsg.pdf`.

[17] Sparkfun. *"Fully Integrated, Hall Effect-Based Linear Current Sensor with 2.1 kVRMS Voltage Isolation and a Low-Resistance Current Conductor"*, 2007. URL `https://www.sparkfun.com/datasheets/BreakoutBoards/0712.pdf`.

[18] Coilcraft. *"Current Sense Transformers CST7030"*, 2017. URL `https://www.coilcraft.com/pdfs/cst7030.pdf`.

[19] Texas Instruments. *"OPAx350 High-Speed, Single-Supply, Rail-to-Rail Operational Amplifiers MicroAmplifier Series"*, 2015. URL `http://www.ti.com/lit/ds/sbos099d/sbos099d.pdf`.

[20] ON Semiconductor. *"RB751V40T1G Schottky Barrier Diode"*, 2014. URL `https://www.onsemi.com/pub/Collateral/RB751V40T1-D.PDF`.

[21] Coilcraft. *"Coupled Chip Inductors PFD3215"*, 2012. URL `https://www.coilcraft.com/pdfs/pfd3215_flyback.pdf`.

[22] More Prachi Gopalrao and A.A. Yadav. *"A Survey on RF Power Amplifier Designing with CMOS Technology"*, International Journal of Computer Applications, ACCNet, 2016.

[23] Matt Ozalas. *"How to Design an RF Power Amplifier: The Basics"*, Keysight Technologies, 2015. URL `https://www.keysight.com/upload/cmc_upload/All/9Apr15WebcastSlides.pdf`.

[24] Lukasz Roslaniec and David J. Perreault. *"Design of Variable-Resistance Class E Inverters for Load Modulation"*, IEEE Energy Conversion Congress and Exposition, 2012.

[25] José Alberto, Ugo Reggiani, and Leonardo Sandrolini. *"Magnetic Near Field from an Inductive Power Transfer System Using an Array of Coupled Resonators"*, 7th Asia Pacific International Symposium on Electromagnetic Compatibility, 2016.

[26] B. Wang, W. Yerazunis, and K. H. Teo. *"Wireless power transfer: Metamaterials and array of coupled resonators"*, Proceedings of the IEEE, vol. 101, pp. 1359-1368, 2013.

[27] E. Shamonina and L. Solymar. *"Magneto-inductive waveguide devices"*, IEE Proc.-Microw. Antennas Propag., Vol. 153, No. 2, 2006.

[28] C. J. Stevens. *"Magnetoinductive waves and wireless power transfer"*, IEEE Transactions on Power Electronics, vol. 30, pp. 6182-6190, 2015.

[29] W. X. Xhong, C. K. Lee, and S. Y. Hui. *"Wireless Power Domino-Resonator Systems With Noncoaxial Axes and Circular Structures"*, IEEE Transactions on Power Electronics, Vol. 27, No. 11, 2012.

[30] B. Wang, D. Ellstein, and Teo K. H. *"Analysis on Wireless Power Transfer to Moving Devices Based on Array of Resonators"*, 6th European Conference on Antennas and Propagation, 2011.

[31] Fei Zhang and Steven A. Hackworth. *"The Relay Effect on Wireless Power Transfer Using Witricity"*, IEEE, 2010.

[32] S. Afdollah, H. Bahrami, M. Sawan, and B. Gosselin. *"A Smart Multicoil Inductively Coupled Array for Wireless Power Transmission"*, IEEE Transactions on Industrial Electronics, Vol. 61, No. 11, 2014.

Appendix A

PCB design and evaluation

A.1 Version 1

Schematic, layout design and BOM for the first version of the sensing board.

A.1.1 Schematic

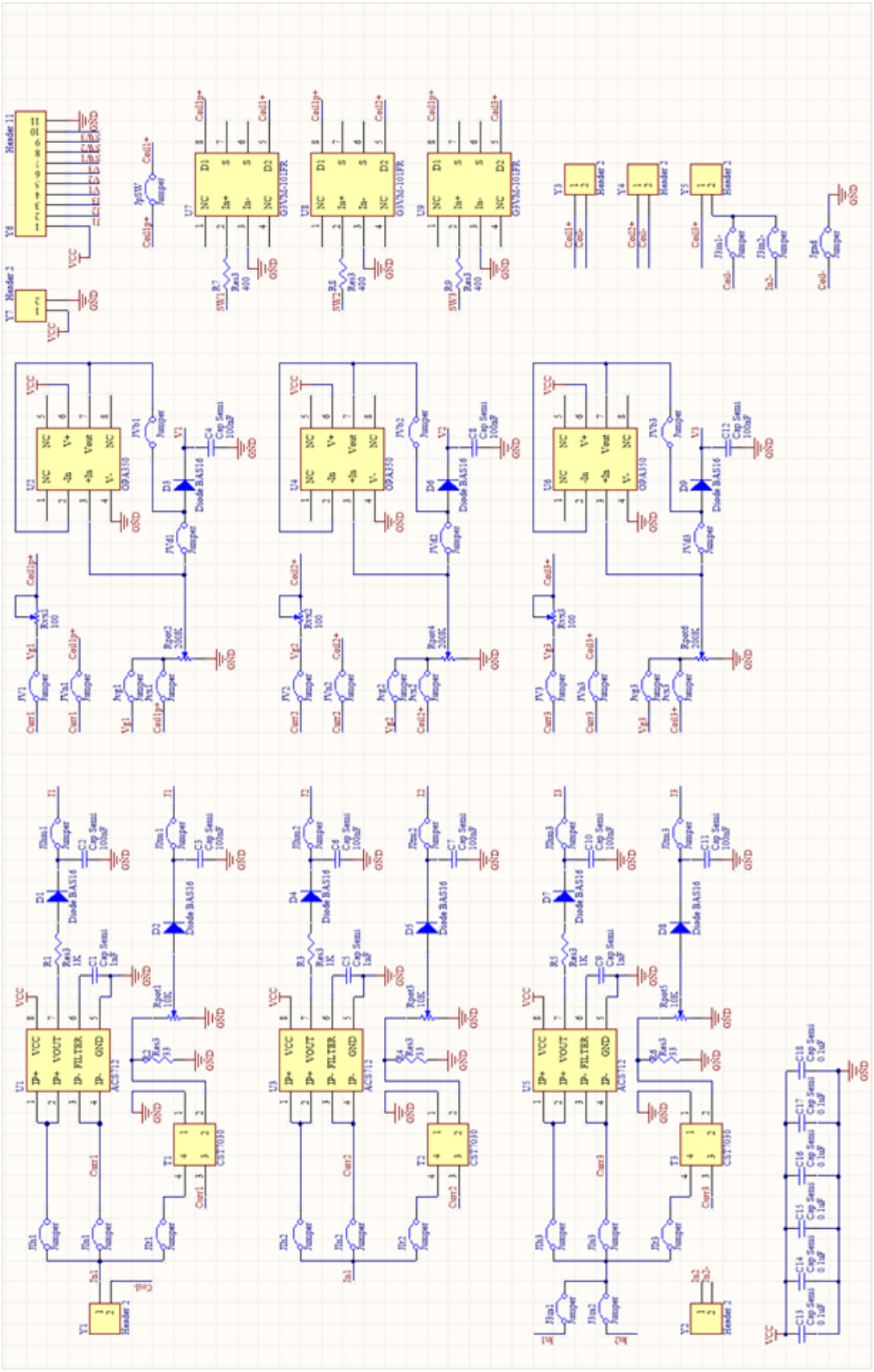

Figure A.1: Schematic used for the first PCB design

A.1.2 Layout

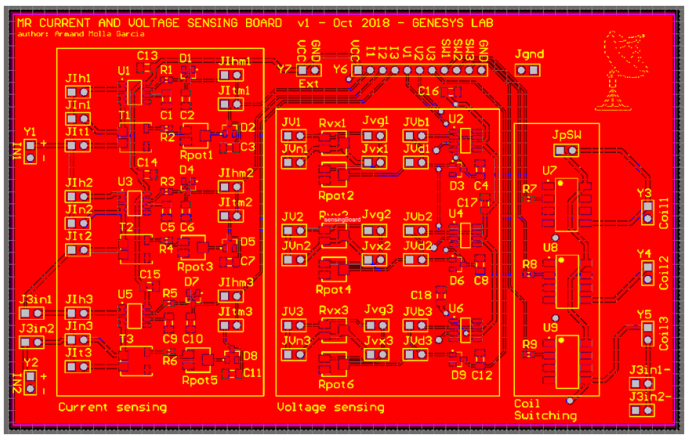

Figure A.2: Top layer view layout design

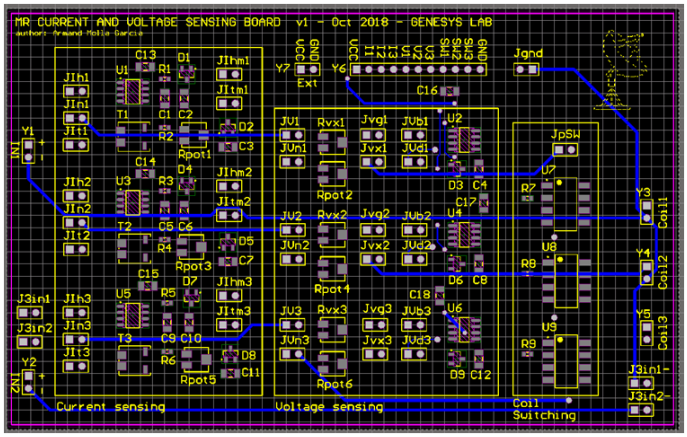

Figure A.3: Bottom layer view layout design

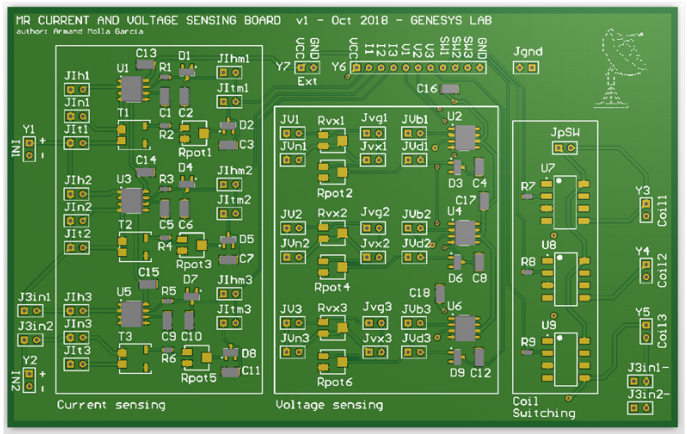

Figure A.4: 3D view

A.1.3 BOM

Item	Qty	Schematic reference	Value	Description
1	6	C13, C14, C15, C16, C17, C18	0,1 uF	Multilayer Ceramic Capacitors 1206
2	6	C1, C5, C9	1 nF	Multilayer Ceramic Capacitors 1206
3	6	C2, C3, C4, C6, C7, C8, C10, C11, C12	33 nF	Multilayer Ceramic Capacitors 1206
4	3	R1, R3, R5	1K ohm	Thick film resistor SMD 0603
5	3	R2, R4, R6	33 ohm	Thick film resistor SMD 0603
6	3	R7, R8, R9	390 ohm	Thick film resistor SMD 0603
7	3	Rpot1, Rpot3, Rpot5	1 Kohm	Square Trimming Potentiometer SM 4mm
8	3	Rpot2, Rpot4, Rpot6	200 Kohm	Square Trimming Potentiometer SM 4mm
9	3	Rvx1, Rvx2, Rvx3	100 ohm	Square Trimming Potentiometer SM 4mm
10	3	T1, T2, T3		CST7030 - current sense transformer
11	3	U1, U3, U5		ACS712 - hall current sensor
12	3	U2, U4, U6		OPA350 - 32MHz operational amplifier
13	3	U7, U8, U9		G3VM-101FR - optocoupler
14	9	D1, D2, D3, D4, D5, D6, D7, D8, D9		Shotcky diode 20V
15	45	J3in1, J3in1-, J3in2, J3in2-, Jgnd, JIh1, JIh2, JIh3, JIhm1, JIhm2, JIhm3, JIn1, JIn2, JIn3, JIt1, JIt2, JIt3, JItm1, JItm2, JItm3, JpSW, JV1, JV2, JV3, JVb1, JVb2, JVb3, JVd1, JVd2, JVd3, Jvg1, Jvg2, Jvg3, JVn1, JVn2, JVn3, Jvx1, Jvx2, Jvx3, Y1, Y2, Y3, Y4, Y5, Y7		2-pin header (jumpers)
16	1	Y6		11-pin header

Table A.1: Sensing board v1 BOM

A.2 Version 2

Schematic, layout design and BOM for the second version of the sensing board.

A.2.1 Schematic

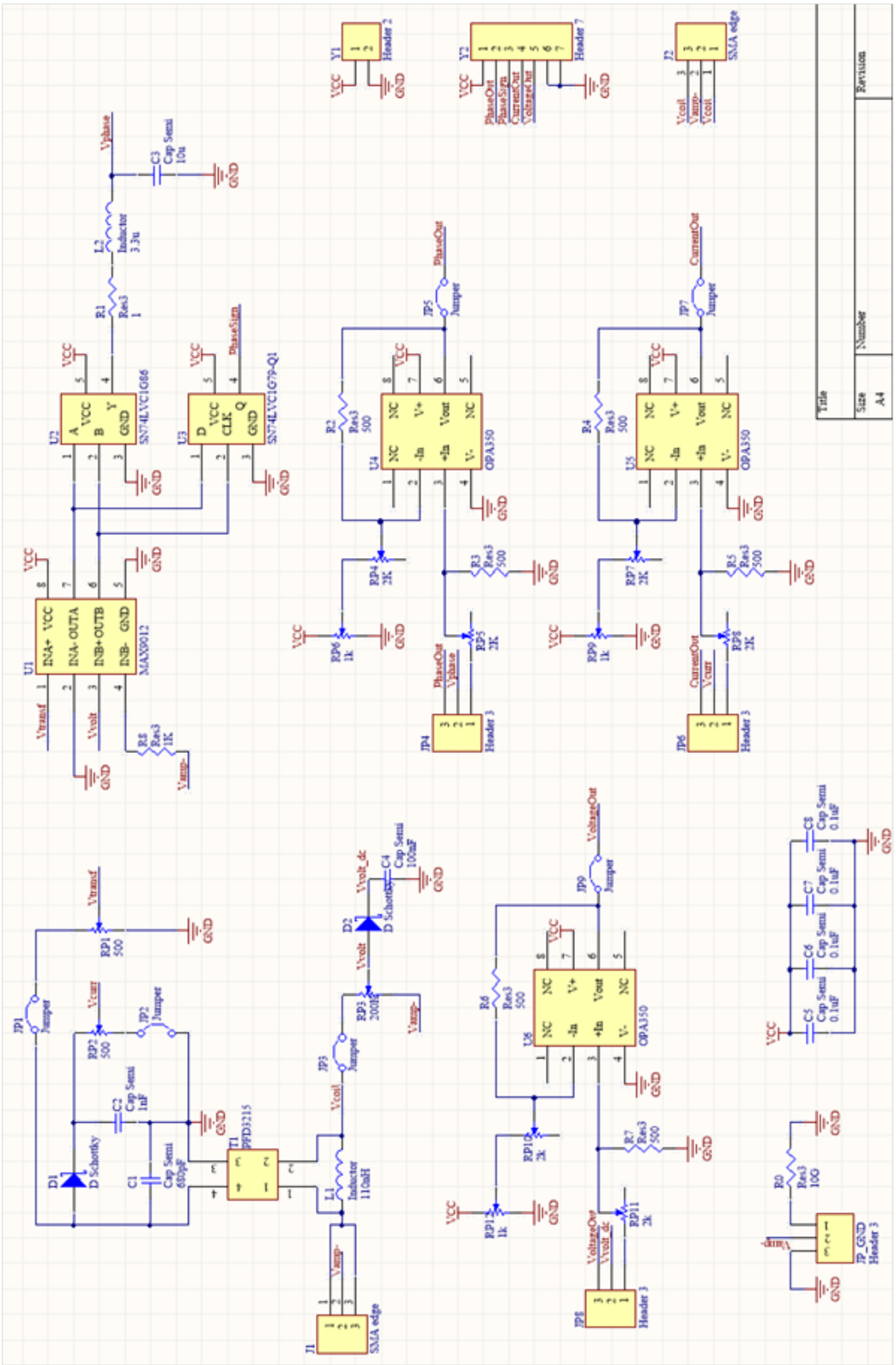

Figure A.5: Schematic used for the second PCB design

A.2.2 Layout

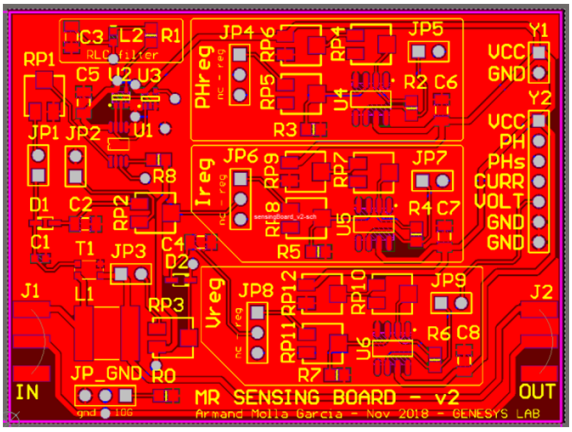

Figure A.6: Top layer view layout design

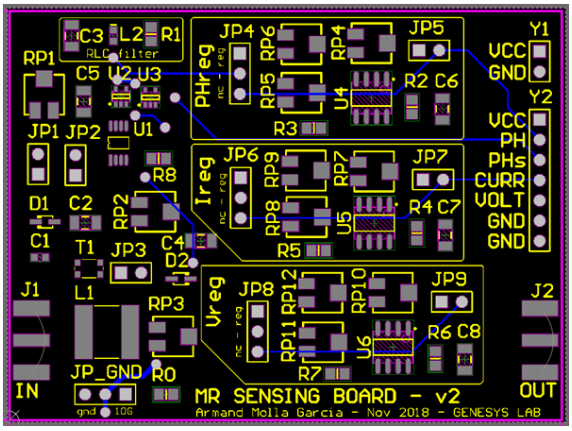

Figure A.7: Bottom layer view layout design

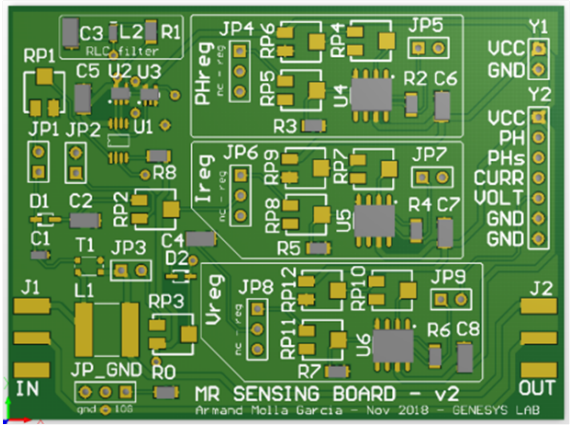

Figure A.8: 3D view

A.2.3 BOM

Item	Qty	Schematic reference	Value	Description
1	4	C5, C6, C7, C8	0,1 uF	Multilayer Ceramic Capacitors 1206
2	1	C2	1 nF	Multilayer Ceramic Capacitors 1206
3	1	C4	33 nF	Multilayer Ceramic Capacitors 1206
4	1	C3	10 uF	Multilayer Ceramic Capacitors 1206
5	1	C1	680 pF	Multilayer Ceramic Capacitors 0603
6	1	L1	110 nH	Fixed Inductors 2222SQ Air
7	1	L2	3,3 uH	Fixed Inductors 0603LS
8	1	R0	10 Gohm	Thick Film Resistors
9	1	R1	1,15 ohm	Thick Film Resistors
10	6	R2,R3,R4,R5, R6,R7	500 ohm	Thin Film Resistors
11	3	RP1, RP2, RP6, RP9,RP12	1 Kohm	Square Trimming Potentiometer SM 4mm
12	1	RP3	200 Kohm	Square Trimming Potentiometer SM 4mm
13	6	RP4, RP5, RP7, RP8, RP10, RP11	2 Kohm	Square Trimming Potentiometer SM 4mm
14	1	T1		PFD3215 1:1 tramsformer
15	1	U1		MAX9012 dual comparator
16	1	U2		SN74LVC1G86 2-input XOR logic gate
17	1	U3		SN74LVC1G79-Q1 flip flop
18	3	U4, U5, U6		OPA350 - 32MHz op amp
19	2	D1, D2		Schottky Diodes 40V 200mW RB751V40T1G
20	6	Y1, JP1, JP2, JP3, JP5, JP7, JP9		2-pin header
21	4	JP_GND, JP4, JP6, JP8		3-pin header
22	1	Y2		7-pin header
23	2	J1,J2		SMA edge connector

Table A.2: Sensing board v2 BOM

A.3 Arduino code

Simple Arduino code used for the averaged measurements. It would compute the average every 1000 samples taken by the ADC.

```
1
#include <stdio.h>
3 #include <math.h>

5 //pins and variables
int anRead = 2;
7 const float SAMPLES = 10000;
int i = 1;
9 float values = 0;
float average = 0;
11


13 // the setup routine runs once when you press reset:
void setup() {
15   // initialize serial communication at 9600 bits per second:
   Serial.begin(9600);
17   //pins setup
   pinMode(anRead, INPUT);
19 }

21 // the loop routine runs over and over again forever:
void loop() {
23

   values = 0;
25   for(i=0;i<(SAMPLES-1);i++){
     values = values + ((float)analogRead(anRead)*5/1024);
27   }
   average = values/SAMPLES;
29

   Serial.println(average);
31 }
```

frame

Appendix B

Amplifier and Beamforming Matlab codes

B.1 Matlab variable load equations computation

```
%% MATLAB calculations for Class-E amplifier parameters
% Tunning following the 2012 paper from Lukasz Roslaniec
% for variable load operation

%% Design variables
f0 = 6.78e6;
Pout = 20;
Rmin = 8;
Kload = 10;          %times that Rmax is bigger than Rmin
Rmax = Kload*Rmin;
Rout = Rmin;         %rated output resistance equals the minimum value
Cdev = 110e-12;      %EPC1007 power transistor capacitance

%% Circuit parameters calculation

Vout_rms = sqrt(Pout*Rout)
Iout_rms = Pout/Rout;
Vdc = Vout_rms/1.15

%% Resonant LCs design

% Ls and Cs resonating at f0, Qs=5, filter for minimum load
% since 5 = (sqrt(Ls/Cs))/Rmin, then
Qs = 5;
Cs = 1/(2*pi*f0*Qs*Rout)
Ls = Qs^2*Rout^2*Cs

% Lp and Cp also resonant at f0, here Qp=5 again
% Parallel tank will filter for the highest load Rmax
Qp = 5;
```

```
Lp = Rmax/(2*pi*f0*Qp)
Cp = (Qp^2*Lp)/Rmax^2

% Lf and Cf calculation to resonate at 1.5*f0
% Characteristic input impedance Zchar of the Lf-Cf SW calculated
% Factor k from simulations, 0.7 optimum here (0.5 to 1.5)
ff = 1.5*f0;
Zchar = 8.75;
Cf = 1/(2*pi*ff*Zchar);
Lf = Cf*Zchar^2
Cadd = Cf-Cdev
```

frame

B.2 Beamforming equations in Matlab

Calculation of the beamforming weights for a simple two-coil beamforming experiment. The input variables read by an Arduino are the voltages at the transmitting coils.

```

clear all;
close all;
clc;

% system variables
f_1 = 2E6; % resonant frequency
omega = 2*pi*f_1;
R_T = 150; % transmitter side intrinsic impedance
R_R = 150; % % receiver side load impedance
V_max1 = 3; % voltage coil1
V_max2 = 3; % voltage coil2
phase_1 = pi/2;
phase_2 = -pi/2;

a=arduino('com3','uno');       %connect to arduino


% arduino readings averaging
while(1)


reading1_1 = readVoltage(a,'A0'); %get voltage arduino
%pause(0.2);
reading1_2 = readVoltage(a,'A0');
%pause(0.2);
reading1_3 = readVoltage(a,'A0');
%pause(0.2);
reading1_4 = readVoltage(a,'A0');
%pause(0.2);
reading1_5 = readVoltage(a,'A0');
```

```
%pause(0.2);
reading2_1 = readVoltage(a,'A1'); %get voltage arduino
%pause(0.2);
reading2_2 = readVoltage(a,'A1');
%pause(0.2);
reading2_3 = readVoltage(a,'A1');
%pause(0.2);
reading2_4 = readVoltage(a,'A1');
%pause(0.2);
reading2_5 = readVoltage(a,'A1');

reading1 = ((reading1_1+reading1_2+reading1_3+reading1_4+reading1_5)/5)
reading2 = ((reading2_1+reading2_2+reading2_3+reading2_4+reading2_5)/5)

%% mutual inductance between transmitters not calculated as it appeared to
    ↪ be negligible
%% mutual inductance between tx and rx & tx currents
V_1 = V_max1 - (reading1*2.15); % tx1 voltage
V_2 = V_max2 - (reading2*2); % tx2 voltage

Z_1 = V_max1/(V_1/R_T); % tx1 impedance
Z_2 = V_max2/(V_2/R_T); % tx2 impedance

M_1 =sqrt(((Z_1-R_T)*R_R)/omega^2); % mutual inductance between tx1 and rx
M_2 =sqrt(((Z_2-R_T)*R_R)/omega^2); % mutual inductance between tx2 and rx

I_1 = V_1/R_T; % tx1 current
I_2 = V_2/R_T; % tx2 current
%% channel estimators
m_1 = omega*M_1/R_R;
m_2 = omega*M_2/R_R;

% weights calculation
sum_m = abs(m_1)^2+ abs(m_2)^2;
beta_1 = m_1/sum_m
beta_2 = m_2/sum_m
%% calculate tx currents, then the voltages to be applied to each of them
I_T_1 = beat_1*I_1; % weighed current for tx1
I_T_2 = beat_2*I_2; % weighed current for tx2
I_L = m_1*I_T_1+m_2*I_T_2; % % estimated rx current

V_T_1 = R_T*I_1+I_L*omega*M_1; % weighed voltage for tx1
V_T_2 = R_T*I_1+I_L*omega*M_2; % weighed voltage for tx2

pause (3)

end
```

frame